Article

Current Biology

Origin and Health Status of First-Generation Africans from Early Colonial Mexico

Highlights

- Genomic and isotopes data suggest an African origin for the three individuals
- One ~14X *Treponema pallidum* sub. *pertenue* genome was recovered
- One ~1,500X hepatitis B virus genome was recovered
- Both pathogen genomes cluster together with present day pathogens from Africa

Authors

Rodrigo Barquera, Thiseas C. Lamnidis, Aditya Kumar Lankapalli, ..., Denise Kühnert, Lourdes Márquez-Morfín, Johannes Krause

Correspondence

kuehnert@shh.mpg.de (D.K.), rlmorfin@gmail.com (L.M.-M.), krause@shh.mpg.de (J.K.)

In Brief

Barquera et al. analyze individuals from a colonial period burial from Mexico. Using an interdisciplinary approach, they reconstruct the genetic ancestry, origins, and health status of three enslaved Africans. Genomes of pathogens recovered from them provide insight on infectious diseases brought to the Americas by the transatlantic slave trade.

Barquera et al., 2020, Current Biology *30*, 2078–2091
June 8, 2020
https://doi.org/10.1016/j.cub.2020.04.002

CellPress

CellPress

Current Biology

Article

Origin and Health Status of First-Generation Africans from Early Colonial Mexico

Rodrigo Barquera,[1,2,13] Thiseas C. Lamnidis,[1,13] Aditya Kumar Lankapalli,[1,13] Arthur Kocher,[3,13] Diana I. Hernández-Zaragoza,[2,4,13] Elizabeth A. Nelson,[1,5] Adriana C. Zamora-Herrera,[6] Patxi Ramallo,[7,8] Natalia Bernal-Felipe,[9] Alexander Immel,[1,10] Kirsten Bos,[1] Víctor Acuña-Alonzo,[2] Chiara Barbieri,[11,12] Patrick Roberts,[7] Alexander Herbig,[1] Denise Kühnert,[3,*] Lourdes Márquez-Morfín,[6,*] and Johannes Krause[1,14,*]

[1]Department of Archaeogenetics (DAG), Max-Planck Institute for the Science of Human History (MPI-SHH), Kahlaische Str. 10, 07745 Jena, Germany

[2]Molecular Genetics Laboratory, Escuela Nacional de Antropología e Historia (ENAH), Periférico Sur y Zapote s/n. Col. Isidro Fabela, Tlalpan, 14030 Mexico City, Mexico

[3]Transmission, Infection, Diversification & Evolution Group (TIDE), Max-Planck Institute for the Science of Human History (MPI-SHH), Kahlaische Str. 10, 07745 Jena, Germany

[4]Immunogenetics Unit, Técnicas Genéticas Aplicadas a la Clínica (TGAC), Calz. del Hueso 714, Coapa, Los Sauces, Coyoacán, 04940 Mexico City, CDMX, Mexico

[5]Institute for the Archaeological Sciences, University of Tübingen, Geschwister-Scholl-Platz, 72074 Tübingen, Germany

[6]Osteology Laboratory, Post Graduate Studies Division, Escuela Nacional de Antropología e Historia (ENAH), Periférico Sur y Zapote s/n. Col. Isidro Fabela, Tlalpan, 14030 Mexico City, Mexico

[7]Department of Archaeology (DA), Max-Planck Institute for the Science of Human History (MPI-SHH), Kahlaische Str. 10, 07745 Jena, Germany

[8]Faculty of Medicine and Nursing, University of the Basque Country (UPV/EHU), Arriola Pasealekua, 2, 20018 Donostia, Gipuzkoa, Spain

[9]Escuela Nacional de Antropología e Historia (ENAH), Periférico Sur y Zapote s/n. Col. Isidro Fabela, Tlalpan, 14030 Mexico City, Mexico

[10]Institute of Clinical Molecular Biology, Kiel University, Rosalind-Franklin-Straße 12, 24105 Kiel, Germany

[11]Department of Linguistic and Cultural Evolution (DLCE), Max-Planck Institute for the Science of Human History (MPI-SHH), Kahlaische Str. 10, 07745 Jena, Germany

[12]Department of Evolutionary Biology and Environmental Studies, University of Zurich, Winterthurerstrasse 190, 8057 Zürich, Switzerland

[13]These authors contributed equally

[14]Lead Contact

*Correspondence: kuehnert@shh.mpg.de (D.K.), rlmorfin@gmail.com (L.M.-M.), krause@shh.mpg.de (J.K.)

https://doi.org/10.1016/j.cub.2020.04.002

SUMMARY

The forced relocation of several thousand Africans during Mexico's historic period has so far been documented mostly through archival sources, which provide only sparse detail on their origins and lived experience. Here, we employ a bioarchaeological approach to explore the life history of three 16th century Africans from a mass burial at the San José de los Naturales Royal Hospital in Mexico City. Our approach draws together ancient genomic data, osteological analysis, strontium isotope data from tooth enamel, $\delta^{13}C$ and $\delta^{15}N$ isotope data from dentine, and ethnohistorical information to reveal unprecedented detail on their origins and health. Analyses of skeletal features, radiogenic isotopes, and genetic data from uniparental, genome-wide, and human leukocyte antigen (HLA) markers are consistent with a Sub-Saharan African origin for all three individuals. Complete genomes of *Treponema pallidum* sub. *pertenue* (causative agent of yaws) and hepatitis B virus (HBV) recovered from these individuals provide insight into their health as related to infectious disease. Phylogenetic analysis of both pathogens reveals their close relationship to strains circulating in current West African populations, lending support to their origins in this region. The further relationship between the treponemal genome retrieved and a treponemal genome previously typed in an individual from Colonial Mexico highlights the role of the transatlantic slave trade in the introduction and dissemination of pathogens into the New World. Putting together all lines of evidence, we were able to create a biological portrait of three individuals whose life stories have long been silenced by disreputable historical events.

INTRODUCTION

Almost 500 years ago, in 1518, Charles I of Spain issued an authorization to transport the first African slaves into the Viceroyalty of New Spain (which at its zenith comprised the entirety of present day Mexico, the Caribbean, parts of the United States and Canada, and all Central America except for Panama) [1]. 5 centuries later, the ancestry of those hundreds of thousands of forcefully abducted people has formed an integral part of the genetic heritage carried by a large number of people in Mexico and a highly visible part of its national cultural heritage. Slavery was the primary mechanism of immigration of Africans to Mexico

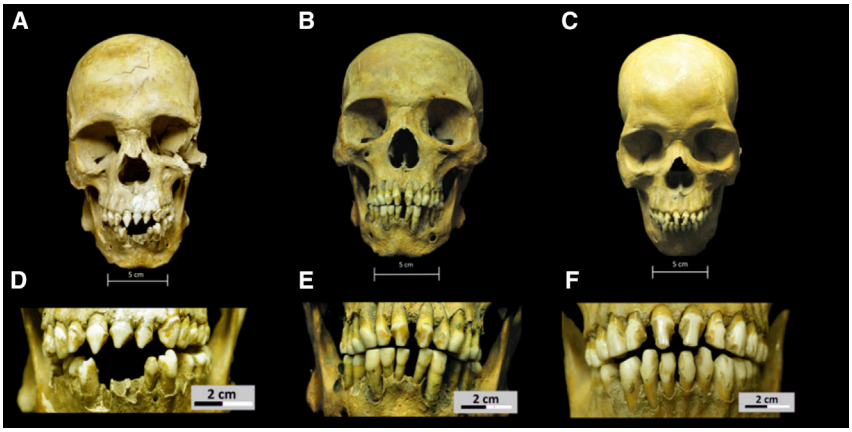

Figure 1. Skulls and Dental Decoration Patterns for the Three African Individuals from the San José de los Naturales Royal Hospital

(A) Skull from individual 150 (SJN001).
(B) Skull from individual 214 (SJN002).
(C) Skull from individual 296 (SJN003).
(D) Close up of dental modification patterns for individual 150 (SJN001).
(E) Close up of dental modification patterns for individual 214 (SJN002).
(F) Close up of dental modification patterns for individual 296 (SJN003).
The skeletons of these individuals are part of the collection of San José de los Naturales, guarded at the Osteology Laboratory of the Post Graduate Studies Division at the National School of Anthropology and History (ENAH), Mexico City, Mexico. Photographs: R. Barquera and N. Bernal.

during the first half of the colonial period, which constitutes one of the most significant forced oppressive migrations in human history [2]. The increased demand for enslaved manual laborers, together with the establishment of the first European settlements in what is euro-centrically referred to as the "New World," caused the growth and consolidation of the transatlantic slave trade. Despite uncertainties around absolute numbers, an estimated 10.6 to 19.4 million Africans had been forcibly deported from their homelands until slavery was finally abolished in most parts of the Americas in the 1860s. To add to these staggering figures, high mortality rates during their voyages meant that only 9.6 to 15.5 million actually arrived in the Americas [3–6]. These data include only the entries through the official ports, which ignores individuals that were smuggled, for whom there is no reliable record. In the case of the Viceroyalty of New Spain, between 130,000 and 150,000 Africans had arrived by 1779, the year in which the importation of slaves into New Spain was banned [7, 8]. Of these, approximately 70,000 entered between the years 1600 and 1640 [3]. The sudden increase in demand was in part due to a reduction in the indigenous labor force that resulted from both casualties in the many conflicts during the European conquest and from diseases (among them, smallpox, measles, and typhoid fever) [9–11] that devastated nearly 90% of the native population [10]. Creoles, Africans, mulattoes, and other African-descended groups were thought to have higher resistance to these diseases compared to Indigenous Americans and Europeans [7, 12–14] making them desirable assets. Further to this, *Las Leyes Nuevas* (The New Laws) of 1542 prohibited the use of Native American labor as slaves in New Spain [15].

The African genetic diversity has been studied in other regions of the Americas by means of genome-wide analysis of both ancient [16–18] and present-day [19, 20] populations. To better understand the lives and health status of first-generation African slaves in Colonial Mexico, historical, archaeological, isotopic, and genetic evidence needs to be considered. Here, we use a bioarchaeological approach that marries ancient human genetic data with osteological analyses, stable carbon and nitrogen isotope analysis, strontium isotope analysis, ethnohistorical information, as well as a molecular screening for potential pathogens to comment on the origins, health status, and life history of three putatively enslaved Africans from Mexico City from a mass burial at the *Hospital Real de San José de los Naturales* (San José de los Naturales Royal Hospital [SJN]) [10, 21]. Documentary evidence indicates this hospital serviced exclusively *los naturales* (i.e., the indigenous population) [22]; however, different sources and studies point to non-indigenous peoples as being treated and buried there [23–27]. Particular traits, such as culturally associated dental modification patterns (Figure 1; see also [6, 28]), suggested a possible African origin of three individuals. Indeed, our results confirm and characterize their African ancestry. We got important insights into these individuals' health status and retrieved genomic material of two pathogens phylogenetically linked to strains from Sub-Saharan Africa. Based on isotopic evidence, we can suggest a non-Mexican origin for these individuals, as they are presumably first-generation enslaved Africans who died very early during the colonial period in Mexico.

RESULTS

Samples were processed according to protocols designed for ancient DNA work in dedicated facilities. We were able to extract DNA from tooth dentine powder for all three individuals, which was used for building genomic libraries and producing ~5 million reads for each of them. Pre-processed sequencing data were used for pathogen screening, and PCR reamplified, reconditioned libraries were enriched for human-specific genomic regions or genomes of pathogens. After sequencing the enriched genomic libraries, quality control (QC), population genetics, and pathogen genome reconstruction analyses were carried out.

Ancient DNA Authentication

We observed short average fragment length (~55 bp) and the characteristic increase in cytosine (C) to thymine (T) transitions toward the termini of the DNA fragments that support the presence of authentic ancient DNA (aDNA) in the dataset. Pre-processed sequences were mapped to the human genome assembly GRCh37 (hg19) [29]. For our uracil DNA glycosylase (UDG)-treated libraries, the rate of deamination damage in the first base on the 5′ and 3′ termini were ~7% and 6%, respectively. After enriching for 1,237,207 single-nucleotide polymorphisms (SNPs), we decreased the number of SNPs to place our coverage in the range of that we generated for the ~600,000 SNP positions present in the Human Origins dataset [30], where ~400,000 SNPs for the three enriched libraries

were obtained. Coverage comparisons of X and Y chromosomes SNPs [31] from the 1,240K capture set assigned all three individuals as genetically male. To estimate levels of nuclear contamination in our samples, we used *ANGSD* to measure the rate of heterozygosity of polymorphic sites on the X chromosome [32]. Further to this, a reconstructed mtDNA consensus sequence was used to estimate mtDNA contamination levels using *schmutzi* [33]. Both methods yielded comparable contamination estimates below 2% for all three individuals (Table 1). The pairwise mismatch rates do not support genetic kinship among the three individuals (Table 2).

Characterization of African Ancestry

The carbon ($\delta^{13}C$) and nitrogen ($\delta^{15}N$) measurements of dentine (Table S2) provided values between $-19.9‰$ and $-18.8‰$ ($\delta^{13}C$) and from $13.2‰$ to $10.8‰$ ($\delta^{15}N$). Broadly speaking, those values show that the dietary protein of the three individuals was composed mainly of terrestrial proteins but with a significant portion of C_4 plants and/or marine proteins, consistent with documented diets either in the arid interior or the western coast of West Africa [34]. Unfortunately, it is difficult to distinguish the two kinds of diet due to an absence of associated faunal remains with the individuals that would provide a local ecological "baseline." A comparison between individuals shows higher nitrogen values ($\delta^{15}N = 13.2‰$) for individual SJN001 relative to the other two individuals ($\delta^{15}N = 10.8‰$ and $10.5‰$ for SJN002 and SJN003, respectively). Without any additional contextual information or isotopic data from fauna, it remains challenging to determine the exact nature of their individual diets. Distinguishing these sources has been a consistent problem in African archaeology, where significant C_4 ecosystems coexist in proximity to the coast [35, 36].

Osteological analyses of the three individuals reveal evidence suggesting a life experience of conflict and hardship. Individual *ML8 SL 150* (SJN001) was found with five buck shots and two healing needles (used in traditional medicine) in the thoracic cavity, as well as gunshot wounds. Both SJN001 and SJN003 (*ML8 SLU9B 296*) presented porotic hyperostosis and *cribra orbitalia*, two pathological changes associated with a skeletal response to nutritionally inadequate diets, anemia, parasitic infectious diseases, and blood loss [37–40]. Individual *ML8 San José 214* (SJN002) displayed several skeletal changes associated with intense labor and heavy manual activity, including enthesopathies on the clavicle and scapulae as well as osteophytic lipping on the joint surfaces with some additional joint contour deformation at the sternoclavicular joint of the clavicle. Additionally, he suffered from a poorly aligned complete fracture in the right fibula and tibia, resulting in associated joint changes of the knee, including osteochondritis dissecans of the distal femoral surface with joint contour deformation and associated osteophytic lipping of the articular surface margin. Furthermore, this individual displayed osteoarthrosis of the lumbar vertebrae in addition to signs of deficient oral health and cut marks on the frontal bone.

Skeletal analysis of cranial nonmetric traits (please refer to the STAR Methods section for further information) showed a strong African affinity for all three individuals (macromorphoscopic characteristics: 92.23% for SJN001; 95.24% for SJN002; 91.95% for SJN003). The dental modification patterns (i.e., decoration of the tooth by mechanical modification) are consistent with cultural practices previously reported for African enslaved individuals from different contexts [41, 42] but also observed in groups living in Western Africa today, most notably in the coastal area and nearby regions of equatorial Guinea, Gabon, Cameroon, the Republic of Congo, and the Democratic Republic of the Congo [43]. Uniparental haplogroups and human leukocyte antigen (HLA) haplotypes are representative of Sub-Saharan populations (Table 1). The mitochondrial lineages of the SJN individuals were compared to a set of published mitochondrial genomes from the same three haplogroups (Figure S1). The three mtDNA haplogroups found show their highest frequencies in Western and Central Africa [44], with haplogroup L1b (present in SJN001) concentrated in Western-Central Africa, particularly along the coastal areas [44, 45]; L3d (present in SJN002) being prevalent in western Sub-Saharan Africa [44, 46]; and L3e1 (present in SJN003) being prevalent in the central areas of the continent [44, 47, 48]. Regarding the paternal lineages, all three individuals carried the Y chromosome E3b1a (E-M2) lineage (but not the same haplotypes; Table 1), which is highly prevalent in modern Sub-Saharan populations (particularly in Western Africa) and equatorial Africans and is also the most common lineage among African Americans [49–53]. In order to get a glimpse at the immunogenetic diversity present in these individuals, we carried out immune capture to obtain information on the HLA allelic variation. HLA diversity is helpful in determining the susceptibility and resistance to specific diseases, both infectious and autoimmune. HLA typing poses technical difficulties, and it can be challenging to call HLA alleles from ancient DNA data. For that reason, we enriched the HLA region with an in-solution capture approach (please refer to the STAR Methods section for further detail), yielding 10×–100× coverage for the HLA region. Allele assignation was carried out using Optitype [54], a software specifically developed to deal with short reads coming from ancient DNA data. The HLA haplotypes described here have so far been reported only in African or African-descent populations, like Mozambique, Kenya, South Africa, and African Americans [55–59]. In the case of both HLA haplotypes of SJN001 and haplotype HLA-A*74:01∼B*49:01∼C*07:01∼DRB1*04:05∼DRB4*01:01∼DQA1*03:02∼DQB1*03:02∼DPA1*02:01∼DPB1*13:01, present in SJN002 (Table 1), none of these haplotypes were yet reported in any African populations, but only in mixed ancestry individuals of at least partial African descent [59, 60]. However, the observed *HLA-A∼B∼C* blocks (corresponding to the HLA class I genomic region, functionally devoted to present endogenous peptides to the immune system) have been reported in Sub-Saharan African populations, such as Luo from Kenya [57] and in Rwandan women [61].

Genomic data from the three individuals were merged to 593,124 autosomal SNPs of the Human Origins (HO) dataset [30] for downstream population genetics analyses. To further assess the genetic relationship of these African individuals to present-day populations from Africa, we carried out principal-component analysis (PCA). We first projected the data from the three individuals on PCs calculated on variation from 371 worldwide populations (Figure S2A) and then on variation from 534 individuals from 51 populations from Northern and Sub-Saharan Africa. We found that the SJN individuals cluster together with Sub-Saharan African populations like Mandenka, Mende,

Table 1. Basic QC and Genetic Markers of the Analyzed African Individuals from the Royal Hospital of San José de los Naturales

Library	Sex	Modeled ^{14}C Dating	Damage 1st Base 3′	Damage 1st Base 5′	Called SNPs on HO (Post-merging)	Contamination Estimates (Post-merging)	
						Schmutzi	ANGSD
SJN001.A0102	M	AD 1453–1626	0.0678	0.0751	427,155	0.02 ± 0.01	0.54% ± 0.002%
SJN001.B0102			0.0309	0.0429			
SJN002.A0102	M	AD 1450–1620	0.0710	0.0803	397,342	0.02 ± 0.01	0.44% ± 0.002%
SJN002.B0102			0.0776	0.0882			
SJN003.A0102	M	AD 1436–1472[a]	0.0474	0.0730	446,940	0.02 ± 0.01	0.28% ± 0.002%
SJN003.B0102			0.0443	0.0698			

	Uniparental Markers		HLA Haplotypes								
Individual	mtDNA Haplogroup	Y-Chr Haplogroup	HLA-A	HLA-B	HLA-C	HLA-DRB1	HLA-DRB3/4/5	HLA-DQA1	HLA-DQB1	HLA-DPA1	HLA-DPB1
SJN001	L1b2a	E1b1a1a1c1b | E-M263.2	A*03:01	B*44:10	C*04:01	DRB1*07:01	DRB4*01:01	DQA1*02:01	DQB1*02:01	DPA1*02:01	DPB1*01:01
			A*66:02	B*44:03	C*03:03	DRB1*16:02	DRB5*02:02	DQA1*01:02	DQB1*05:02	DPA1*02:02	DPB1*01:01
SJN002	L3d1a1a	E1b1a1a1d1 | E-P278.1 E-M4254	A*30:01	B*42:01	C*17:01	DRB1*03:02	DRB3*01:01	DQA1*04:01	DQB1*04:02	DPA1*02:01	DPB1*15:01
			A*74:01	B*49:01	C*07:01	DRB1*04:05	DRB4*01:01	DQA1*03:02	DQB1*03:02	DPA1*02:01	DPB1*13:01
SJN003	L3e1a1a	E1b1a1a1c1a1c (E-CTS8030)	A*30:01	B*42:01	C*17:01	DRB1*07:01	DRB4*01:01	DQA1*03:01	DQB1*02:02	DPA1*01:03	DPB1*04:01
			A*66:02	B*58:01	C*07:01	DRB1*15:03	DRB5*01:01	DQA1*01:02	DQB1*06:02	DPA1*01:03	DPB1*02:01

[a]These years refer to pre-contact dates; however, a possible reservoir effect due to marine diet cannot be ruled out as discussed in the Results section.

CellPress

Table 2. Pairwise Mismatch Ratio Analysis

Individual 1	Individual 2	SNPs Tested	Mismatched SNPs	Mismatch Ratio
SJN001	SJN002	594,706	160,514	0.2699
SJN001	SJN003	661,252	178,194	0.2695
SJN002	SJN003	613,943	164,424	0.2678

Wambo, Ovambo, and Damara. When PC1 and PC2 are considered (Figure S2B), the three individuals are projected in the Bantu-speaking population cluster. When plotting PC1 versus PC3 (Figure 2A), the three individuals from SJN appear slightly separated from each other. SJN002 and SJN003 practically overlap with each other and are projected in close proximity to the Wambo population of Southern Africa. SJN001 is projected close to the other two individuals from SJN but falls even closer to the Mende population of Western Africa. PC3 separates hunter-gatherer populations like the Mbuti, Biaka, and Hadza from all other African populations. Admixture estimates (lowest cross validation error at $K = 10$) show that the SJN individuals look very similar, though not identical, in terms of genetic ancestry composition (Figure 2C). Predominantly, ancestry components that are shared with Sub-Saharan populations, such as Yoruba (non-Bantu speakers), Mandenka (non-Atlantic Niger-Congo linguistic family), and Bantu speakers from Kenya and South Africa, were found in all three individuals. An additional component shared with Mbuti and/or Biaka was also evident for SJN002 and SJN003. This extra component might affect the projection of these individuals in the PCA, especially when PC3 is considered. No ancestry related to other continental sources (especially Native Americans) is visible in the ADMIXTURE results (Figure 2C). Altogether, these data support a heterogeneous genetic makeup for the SJN individuals within Sub-Saharan Africa, with clear links to Central-Western Africa and possible links with populations who live in Southern Africa today.

Fine-Scale Population Genetics Analyses

We calculate outgroup F_3 statistics of the form f_3 (outgroup; SJN00X, *Y*) to measure the amount of shared genetic drift of each individual from SJN with a panel of worldwide populations, using the genome of the Ust'-Ishim early modern human from Siberia [62] as an outgroup. Ust' Ishim is a 45,000-year-old Siberian individual that is equally related to both East Asians and West Eurasian hunter-gatherers [62]. This individual represents therefore an outgroup population for West African populations. The highest f_3 values for each individual were with human groups speaking Niger-Congo languages (Figure 3). To test to which specific African population the SJN individuals are most closely related to or shared an excess of alleles with any given population, *D*-statistics of the form *D* (chimp, SJN00X; *X*, target) were used, where target was substituted by the population that gave the highest f_3 value for each individual. For all three individuals from SJN, no population was significantly more closely related to them than to the target population. For SJN001 (Figure S3A), Mende were used as target; for SJN002 (Figure S3B), Bantu-speaking Ovambo were used as target; and for SJN003 (Figure S3C), Lemande were used as target. To test for cladality between each of the individuals from SJN and their respective target populations, we computed *D* statistics of the form *D* (chimp, X; target, SJN00X). We find that none of the ancient individuals are truly cladal with any target population (Table S1). The fact that none of the individuals showed specific genetic affinity with any modern African populations can be due to (1) past migration (i.e., during the colonial period) and/or reallocation of populations, (2) not enough representation of the groups they are more closely related to in the datasets tested, or (3) the populations they are genetically related to do not exist any longer. Interestingly, a recent manuscript [18] described the recovery and characterization of genomic DNA from a tobacco pipe belonging to an African woman that was found to be genetically closely related to present-day Mende from Sierra Leone, which further support Mende-related populations as a source of African genetic ancestry brought into the Americas during the colonial period.

Evidence of the Place of Birth from Strontium Isotope Analysis

Radiocarbon dating suggests that these individuals died shortly after the beginning of the colonial period in Mexico City (Table 1). To further assess the origin of these ancient individuals, we carried out strontium analysis on the molars of each individual, which forms early during childhood and thus is a good proxy for place of birth. For all three individuals, the strontium ratio values are above 0.7089 (SJN001: 0.71078 ± 0.00001; SJN002: 0.72045 ± 0.00001; SJN003: 0.72026 ± 0.00001), which is the highest value recorded for Mexico in the northern part of the Yucatán Peninsula (Tizimin and Dzibilchaltun) [63–65] and even higher than those found for central Mexico (Teotihuacan [0.7049], Xico [0.7045], Chapantongo [0.7052], and Mexico City [0.7062–0.7064]) [63, 66]. In fact, these values are consistent with a West African origin (0.70603–0.74143; Figures 2B and S4; see also [63, 67]).

Paleomicrobiological Findings

The three individuals were buried in a mass grave in the grounds located just outside of the hospital. Their mass grave contained skeletal remains of several individuals disposed in layers, which is consistent with burials made during epidemics, in which dead bodies rapidly outnumber the availability of single graves. We therefore decided to screen these individuals for potential pathogenic agents using a bioinformatic approach [68] to screen and filter reads from the genomic libraries, and this way, we obtained reads mapping to bacteria that could either be part of the oral microbiota (like *Tannerella forsythia*, *Streptococcus mutans*, and *S. gordonii*) or implicated in taphonomic processes (*Clostridium tetani*). Apart from environmental bacteria, 51 reads were mapping specifically to *Treponema pallidum* genomes in individual SJN003, which were marked as potentially positive for treponemal infection. We also found evidence of hepatitis B virus (HBV) DNA in individual SJN001 (library SJN001.B0102), with eight sequencing reads mapping specifically to HBV.

The positive libraries were enriched for HBV (SJN001) and *Treponema pallidum* (SJN003), respectively, using a modified in-solution capture strategy followed by paired-end sequencing (Supplemental Information for further details). After capture, a total of 50,493 (deduplicated) reads mapping to the HBV reference genome were recovered from SJN001. Those exhibited typical patterns of ancient DNA damage, and the complete HBV circular

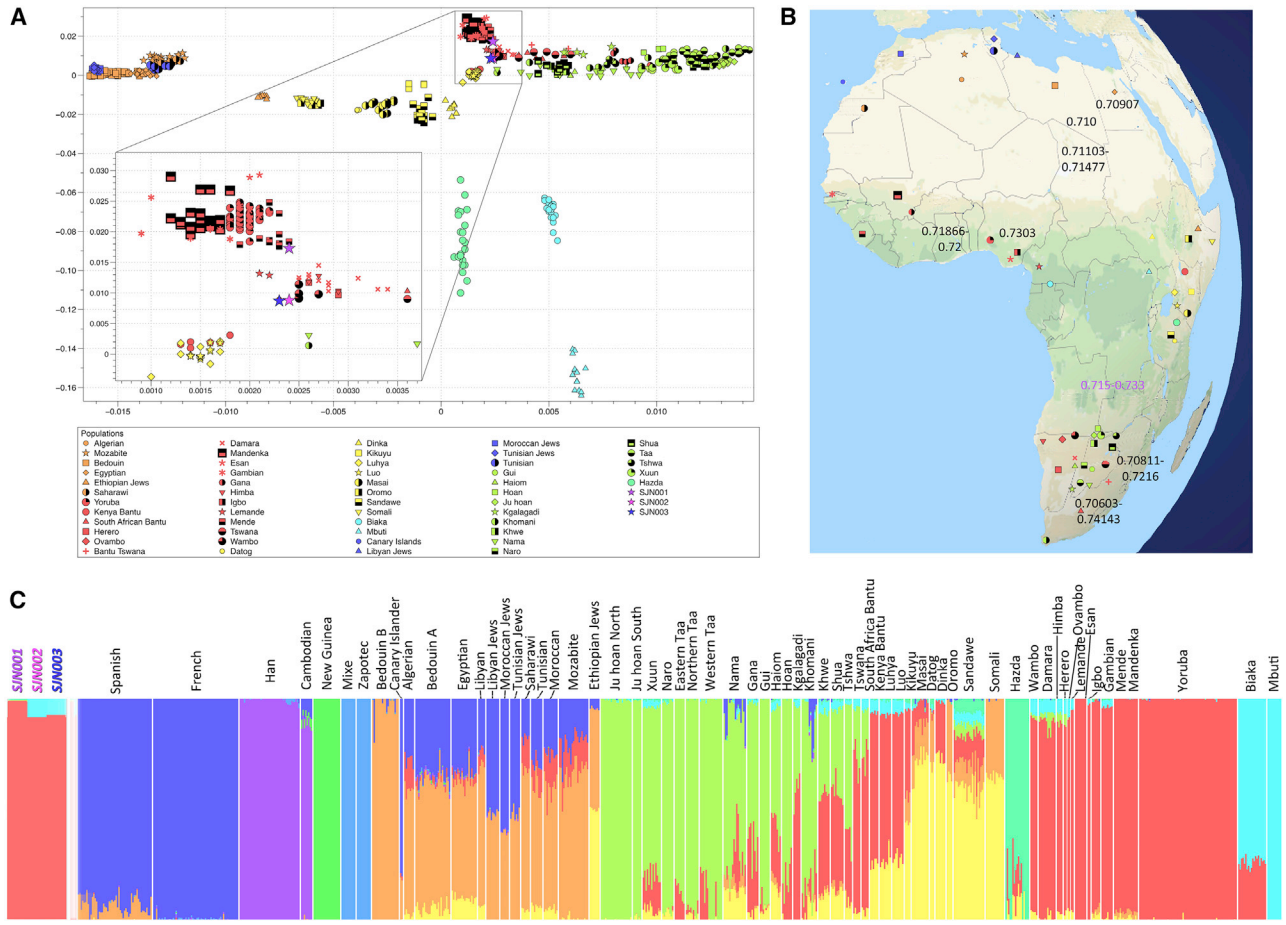

Figure 2. PCA (PC1 versus PC3), Geographic Locations of African Populations Used in the Present Study, and Typical Sr Ratios for Africa

(A) PCA (PC1 versus PC3) showing the genetic relationship of SJN Africans (purple, pink, and violet stars) to Western Africa Niger-Congo linguistic speakers.

(B) Map of Africa showing the places where African populations used for PCA and ADMIXTURE analyses are from. Numbers indicate typical $^{87}Sr/^{86}Sr$ ratios for some regions of Africa (see also Figure S4).

(C) Admixture plot (K = 10) for African populations and potential genetic variation candidate sources due to the demographic history of the Viceroyalty of New Spain (modern Mexico).

genome could be recovered, with a mean coverage of 1,567-fold. These results confirmed that SJN001 was infected with HBV. The ancient HBV genome exhibited a 6-nt insert at the carboxyl end of the core gene, which is characteristic of the HBV A genotype [69]. The phylogenetic analysis confirmed that SJN001 HBV belonged to genotype A (Figure 4) and further showed that it was included in quasi-subgenotype A3 (QS-A3) [70]. Today, QS-A3 is typically found in West Africa. More specifically, SJN001 HBV grouped with strains isolated from Gambia and Guinea.

From SJN003, we reconstructed a *T. pallidum* genome at a mean coverage of 14-fold with 96.66% of the reference genome (Nichols strain) covered at 5-fold average coverage. After aligning the SJN003 genome to previously reported ancient and modern *Treponema pallidum* genomes [71], we produced a maximum likelihood tree (Figure 5) that showed the SJN003 genome to cluster within *Treponema pallidum* subsp. *pertenue* (TPE), the causative agent of yaws. Surprisingly, we found that the SJN003 strain is most closely related to the ancient TPE genome 133 previously isolated from human remains from Colonial Mexico [71]. Both genomes are phylogenetically associated with strains isolated from patients in Ghana.

DISCUSSION

Our combination of genetic analyses, isotope data, ethnohistorical information, and osteobiographies led to the construction of unique life portraits for three individuals from a colonial hospital cemetery in Mexico City. We opted to treat these three individuals independently as opposed to predicating our analysis on the assumption that they represent a singular cultural tradition and ethnic history; this approach was used based on the evidence of forced social intermixing as a means of social control and disintegration among the enslaved population [2, 3, 5, 72]. Osteological assessment, dental modification patterns, and their genetic ancestry are all consistent with a Western or Southern African origin for the three individuals. This finding is further supported by strontium isotope ratios that suggest a non-local origin outside Mexico. The lives of physical hardships and traumas revealed by their osteobiographies, coupled with the fact that most

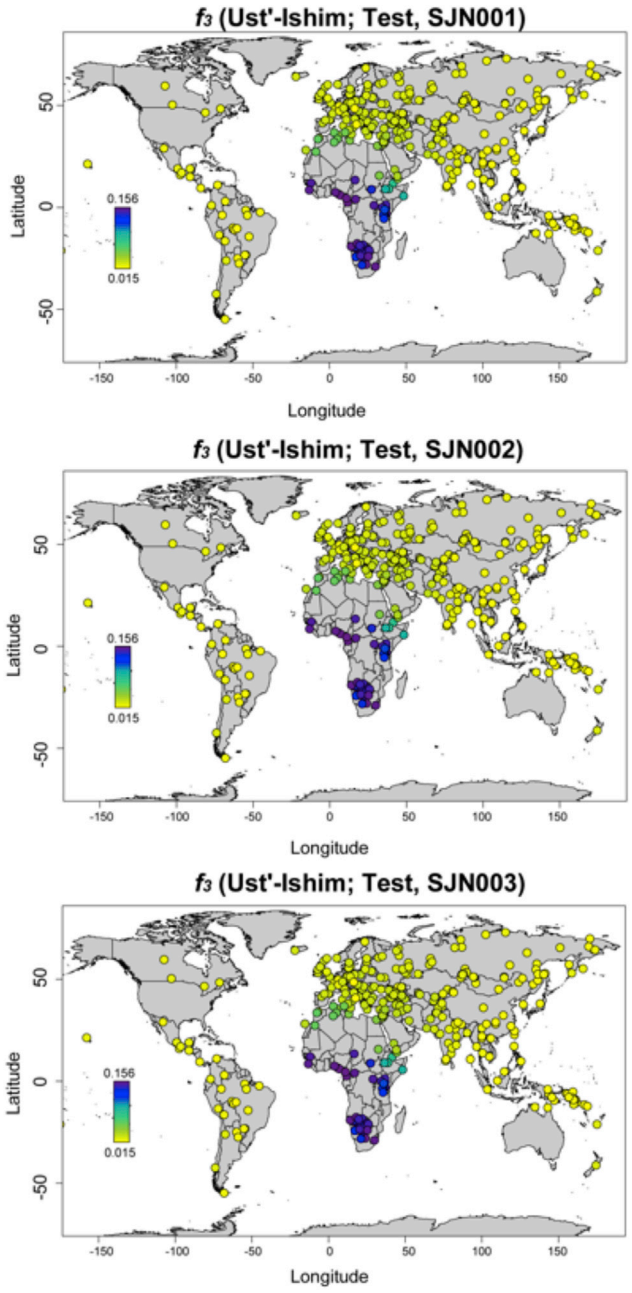

Figure 3. Heatmap of Outgroup f_3 Values for Each Individual from SJN Using a Worldwide Present-Day Population Dataset and Ust'-Ishim as the Outgroup

Higher f_3 values correspond to darker colors.

Sub-Saharan Africans in the Americas from the early colonial period (consistent with SJN individuals' radiocarbon dates) were taken there by force, make the natural conclusion that these individuals were actually enslaved Africans, even in absence of concrete archaeological evidence (such as the individual from the ex-Temple of *Corpus Christi* who was found in shackles) [73].

The genomic analyses suggest that all three individuals show unadmixed African ancestry that is similar to that of Western and Southern African populations. Combining those results with the strontium isotope ratios evidence allows us to conclude that all three individuals were born outside Mexico and likely originate from Western Africa. To the best of our knowledge, they are the earliest genetically identified first-generation Africans in the Americas. mtDNA lineages found in the individuals from SJN (L1 and L3) have been found, although not highly represented, among modern day Mexicans with mixed ancestry [74, 75]. The African HLA haplotypes found in the SJN individuals, or parts of their haplotypes, can be found throughout modern Mexico in frequencies ranging from 0.01% to 2.27% [76]. Alleles HLA-DRB1*07 and HLA-DQB1*02 have been previously found associated with decreased antibody response against HBV and non-responsiveness to HBV vaccination [77, 78]. Interestingly, those two alleles are present in individual SJN001, which was found to be infected with HBV. Those alleles are also present in SJN003 but joined by protective alleles [77, 79], namely HLA-DQB1*06:02 and HLA-DPB1*02:01, which could have aided this individual not to become infected, if he would have been exposed to the virus in the first place. There is currently no reported association between HLA alleles and treponemal infections (apart from HLA-DRB1*14 in Asians) [80]. The fact that three of the six haplotypes were not previously reported in any African population highlights the necessity for exhaustive sampling of HLA haplotypes in African populations. D-statistics identify the closest genetic matches for the three individuals in central West Africa, Western Africa, and Southern African populations (Bantu-speaking groups). Our analyses point to a high genetic diversity in the populations who were the initial sources of the slave trade as suggested by historical records [3, 7, 81]. Furthermore, it is possible that the genetic diversity of living African populations was shaped by substantial migrations through the past four centuries, which displaced human groups and genetic ancestries. The analysis of ancient DNA from early African slave migrants in the Americas therefore provides an alternative opportunity to look at the past genetic makeup of the African continent, where the climatic conditions are not ideal for DNA preservation.

Based on radiocarbon dating, the three individuals lived during the early years of the colonial period in Mexico City (^{14}C range: AD 1436–1626). The osteobiography revealed non-specific markers of physiological stress, evidence of occupational stress and healed severe wounds. They were found in the context of a mass grave (stacked in several layers suggestive of catastrophe deposits made during periods of epidemics) in proximity to a hospital that served only indigenous people [21], from a time period notorious for major epidemics in the region.

Based on our molecular screening, two of the three individuals showed molecular evidence of infectious diseases. HBV is widespread today and poses a significant global health burden [82]. It is currently classified into ten different genotypes that are heterogeneously distributed around the globe [69], and its long history infecting humans dates back at least to the Late Neolithic and Bronze Age [83, 84]. The biogeographic distribution of this virus is tightly linked to human history and migration, given its ease of transmission through contact with infected body fluids and the fact that it can cause a chronic infection [82]. Dispersion of HBV in the past through forced African migration was suggested by the presence of extant African HBV subgenotypes in regions

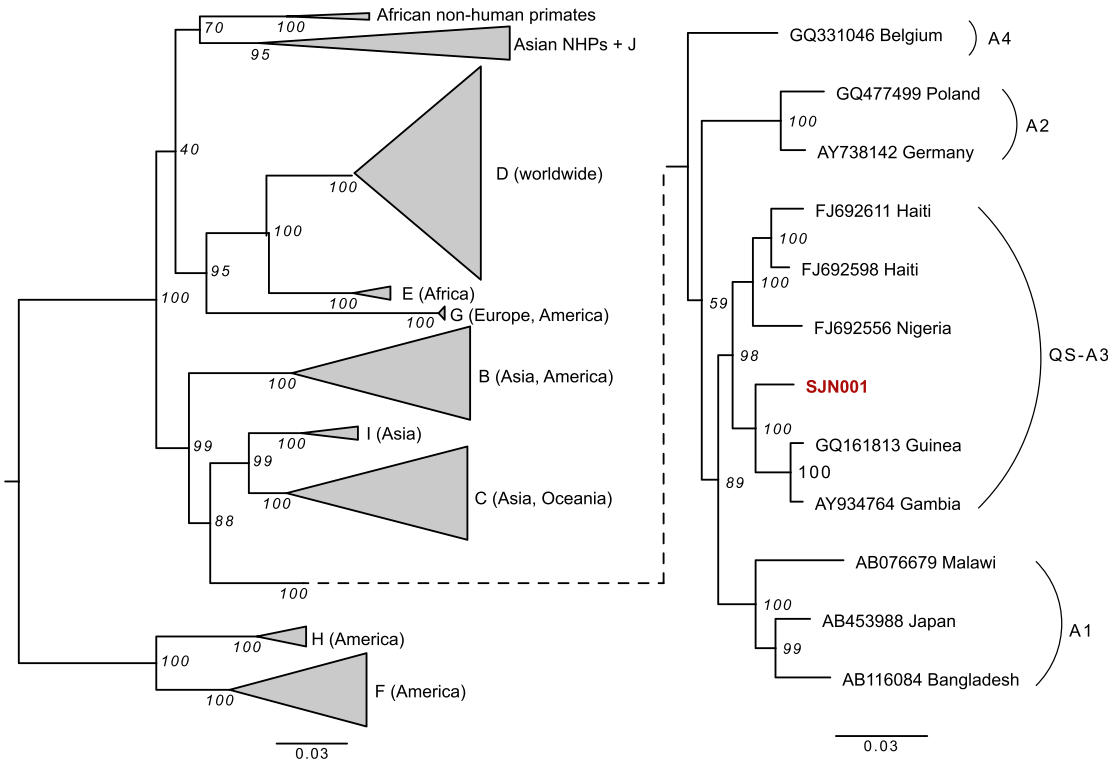

Figure 4. Phylogenetic Tree of Hepatitis B Virus Based on Full Genomes, Including SJN001, Estimated by Maximum Likelihood

Branch lengths represent numbers of substitutions. Bootstrap support values are written at the nodes. In the left panel, inter-genotype relationships are shown and the main continental distribution of each genotype is indicated [69]. The relationships within genotype A and the position of SJN001 are shown in the right panel.

where slavery was practiced [69, 85]. Given that individual SJN001 carried the HBV QS-A3 genotype typically found in West Africa today, coupled with the data that support his origins in this region, provides the first direct evidence of HBV disease movement with a potential dissemination through the transatlantic slave trade. Today, Haiti is the only location outside Africa where the HBV QS-A3 subgenotype is found [69, 85]. Thus, our results reveal that this HBV lineage seems not to have established itself in Mexico.

In contrast, the variety of yaws identified in individual SJN003 shares a common origin with the strain identified in a 17th-century individual of Colonial Mexico City carrying a European mitochondrial haplogroup (H1c+152) [71]. The two strains also cluster with yaws subtypes identified in extant West African groups (although the nodes for the relevant sections of the tree have low statistical support; Figure 5). The osteopathological findings on SJN003 (i.e., cribra orbitalia and hyperostosis and a mild lesion in the frontal bone; please refer to the STAR Methods section for further details) are consistent with chronic infectious diseases and have been reported in suspected cases of individuals affected by treponemal diseases. The polymorphic nature of the lesions left on the bone by treponemal bacteria invites one to pay attention to any potential treponematosis case [71]. These data suggest the establishment of at least one disease of African origin in the local population. As yaws is a highly contagious skin infection that is associated with poor hygiene, it is unsurprising that skeletal signs of treponemal diseases have been reported in other African enslaved individuals from similar historic periods in other contexts in Europe [42]. Our findings add to the discussion of the dynamics of treponemal diseases in the colonial period of Mexico, where they were a prominent yet not completely understood health issue [86, 87]. Our current data, however, shed little light on the reason for their deposition in a presumed epidemic burial ground.

Here, we present the application of a comprehensive set of methods and techniques to display the first in-depth characterization of first-generation African slaves in Colonial Mexico, a historically oppressed group. This was accomplished through reconstruction of the origins and life histories of three putatively enslaved Africans from the beginning of the colonial period in central Mexico. We were able to describe their biological identity and explore elements of their health status by recovering high-quality ancient DNA from both the individuals and their identifiable pathogens. Our work adds important information on the origin, health status, and life histories of the first generation of African slaves that were forcefully relocated and transported to the New World during one of the most horrific cases of callous disregard for human life and violation of human rights during the colonial period. By investigating the origin and disease experience of these individuals through molecular methods and evaluating the skeleton for signs of life experience and cultural affinity, we illuminate, in some measure, the identity, culture, and life of these people whose history has largely been lost. Furthermore, by exploring the African diversity that first came into Mexico and

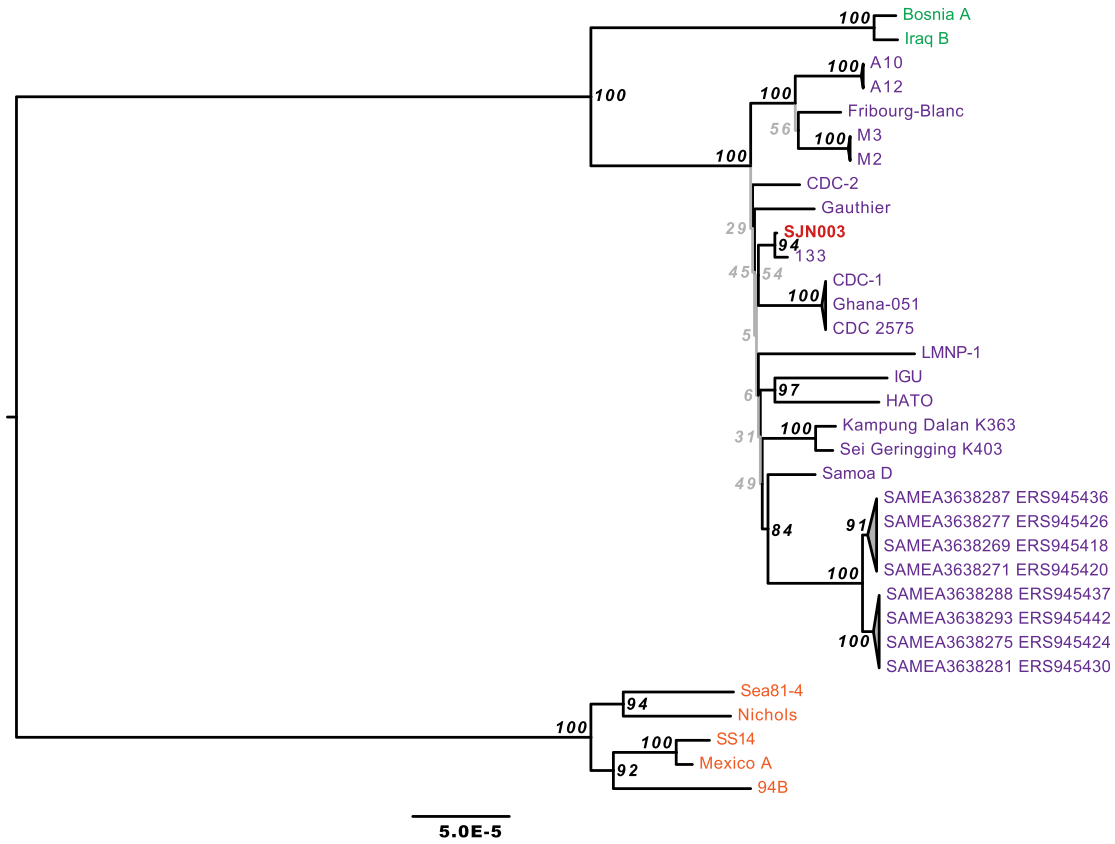

Figure 5. Maximum Likelihood Tree for Ancient Treponemal Genomes from SJN003 (*T. pallidum* sub. *pertenue*), 113 (*T. pallidum* sub. *pertenue*), and 94B SJN003 (*T. pallidum* sub. *pallidum*) and 30 Modern *Treponema pallidum* Genomes

Orange, violet, and green tip labels represent *T. pallidum* subsp. *pallidum* (causative agent of syphilis), *T. pallidum* sub. *pertenue* (causative agent of yaws), and *T. pallidum* sub. *endemicum* (causative agent of bejel) strains, respectively. The scale represents the mean number of substitutions per site for the GTR+GAMMA substitution model. The strain found in individual SJN003 branches with *T. pallidum* sub. *pertenue* strains. Bootstrap support for each branch estimated from 1,000 replicates is provided. The branches with statistical support lower than 80 are presented in gray.

Latin America, we can draw a sharper picture of the biological legacy and cultural roots of modern Latin Americans, explore the extent of this diversity through different disciplines, and also acknowledge how African populations contributed to the biological diversity of mixed ancestry populations of the Americas.

STAR★METHODS

Detailed methods are provided in the online version of this paper and include the following:

- KEY RESOURCES TABLE
- RESOURCE AVAILABILITY
  - Lead Contact
  - Materials Availability
  - Data and Code Availability
- EXPERIMENTAL MODEL AND SUBJECT DETAILS
  - Archaeological sites and sample description
- METHOD DETAILS
  - Osteological assessment
  - Stable isotope analysis, diets, and the reservoir effect
  - Ancient DNA sample processing and quality control
- QUANTIFICATION AND STATISTICAL ANALYSIS
  - QC and data processing for human PopGen
  - Pathogen genomes assemblies

SUPPLEMENTAL INFORMATION

Supplemental Information can be found online at https://doi.org/10.1016/j.cub.2020.04.002.

ACKNOWLEDGMENTS

The authors wish to thank Franziska Aron, Cäcilia Freund, Rita Radzeviciute, Raphaela Stahl, Marta Burri, Antje Wissgott, Guido Brandt, András Szolek, Stephen Clayton, Perla del Carmen Ruíz Albarrán, Laura Curiel Giles, and Bersal del Carmen Villegas Camposeco for their valuable technical and analytical support. We are grateful to Jorge A. Gómez Valdés, Stephan Schiffels, Choongwon Jeong, Arturo Pacho Varela, Kathrin Nägele, Vanessa Villalba, Cosimo Posth, Maria Spyrou, Felix Key, and Maïté Rivollat for insightful comments and helpful discussions, which are part of the finished version of this manuscript. We acknowledge the Council of Archaeology, National Institute of Anthropology and History (INAH) (Mexico City, Mexico) for the permit granted to analyze the individuals from the San José de los Naturales collection (project: *Identificación de los sitios de origen de los individuos con limado dental característico de grupos africanos el Hospital Real de San José de los Naturales a través de análisis genético molecular*; official notice number: 401.B(4)19.2015/36/1026; final report approval: 401.1S.3-2020/0112). C.B

was supported by the University Research Priority Program of Evolution in Action of the University of Zurich. This work was financially supported by the Max Planck Society.

AUTHOR CONTRIBUTIONS

R.B., D.I.H.-Z., N.B.-F., V.A.-A., A.H., D.K., L.M.-M., and J.K. conceived the project. R.B., D.I.H.-Z., N.B.-F., and L.M.-M. performed the registration and photographic recording. R.B., D.I.H.-Z., E.A.N., A.C.Z.-H., and N.B.-F. performed the osteological and paleopathological analyses. R.B., L.M.-M., and J.K. performed the sampling. R.B. performed the lab work. A.I. contributed to the design of the HLA capture. A.H. developed the hepatitis B virus in-solution capture design. P. Roberts and P. Ramallo performed the isotopes analyses. R.B., T.C.L., C.B., and J.K. analyzed the population genetics data. A.K., A.K.L., A.H., D.K., and J.K. assembled, analyzed, and discussed the hepatitis B virus genome and the *Treponema pallidum* sub. *pertenue* genome. All authors discussed the results. R.B., T.C.L., D.I.H.-Z., E.A.N., L.M.-M., and J.K. wrote the paper with contributions from all authors. All authors read and approved the final version. R.B., D.I.H.-Z., N.B.-F., and L.M.-M. wrote and submitted the final report (in Spanish) for the Council of Archaeology (INAH) based on the present manuscript.

DECLARATION OF INTERESTS

The authors declare no competing interests.

Received: January 17, 2020
Revised: March 3, 2020
Accepted: April 1, 2020
Published: April 30, 2020

REFERENCES

1. Lockhart, J., and Schwartz, S. (1983). Early Latin America (Cambridge University Press).
2. Acuña-Alonzo, V. (2005). La contribución genética africana a las poblaciones contemporáneas. PhD thesis (Escuela Nacional de Antropología e Historia).
3. Manning, P. (1993). Migrations of Africans to the Americas: the impact on Africans, Africa, and the New World. Hist. Teacher *26*, 279–296.
4. Lovejoy, P.E. (2011). Esclavitud y comercio esclavista en el África Occidental: investigaciones en curso. In Debates Históricos Contemporáneos: Africanos y Afrodescendientes en México y Centroamérica, M.E. Velázquez, ed. (Centro de Estudios Mexicanos y Centroamericanos), pp. 35–57.
5. Barquera, R., and Acuña-Alonzo, V. (2012). The African colonial migration into Mexico: history and biological consequences. In Causes and Consequences of Human Migration: An Evolutionary Perspective, M.H. Crawford, and B.C. Campbell, eds. (Cambridge University Press), pp. 201–223.
6. Bernal Felipe, N., and Barquera Lozano, R. (2017). Las raíces africanas en México: perspectivas desde la antropología física. In Antropología Física: Disciplina Bio-psico-social, L. González Quintero, and A. Barragán Solís, eds. (Instituto Nacional de Antropología e Historia), pp. 227–250.
7. Aguirre Beltrán, G. (1972). La Población Negra en México: Estudio Etnohistórico, Second Edition (Fondo de Cultura Económica).
8. Lisker, R., Loria, A., and Cordova, M.S. (1965). Studies on several genetic hematological traits of the mexican population. 8. Hemoglobin s, glucose-6-phosphate dehydrogenase deficiency, and other characteristics in a malarial region. Am. J. Hum. Genet. *17*, 179–187.
9. Vågene, Å.J., Herbig, A., Campana, M.G., Robles García, N.M., Warinner, C., Sabin, S., Spyrou, M.A., Andrades Valtueña, A., Huson, D., Tuross, N., et al. (2018). Salmonella enterica genomes from victims of a major sixteenth-century epidemic in Mexico. Nat. Ecol. Evol. *2*, 520–528.
10. Marr, J.S., and Kiracofe, J.B. (2000). Was the huey cocoliztli a haemorrhagic fever? Med. Hist. *44*, 341–362.
11. Burns, J.N., Acuña-Soto, R., and Stahle, D.W. (2014). Drought and epidemic typhus, central Mexico, 1655-1918. Emerg. Infect. Dis. *20*, 442–447.
12. Wang, S., Ray, N., Rojas, W., Parra, M.V., Bedoya, G., Gallo, C., Poletti, G., Mazzotti, G., Hill, K., Hurtado, A.M., et al. (2008). Geographic patterns of genome admixture in Latin American Mestizos. PLoS Genet. *4*, e1000037.
13. Ruiz-Linares, A., Adhikari, K., Acuña-Alonzo, V., Quinto-Sanchez, M., Jaramillo, C., Arias, W., Fuentes, M., Pizarro, M., Everardo, P., de Avila, F., et al. (2014). Admixture in Latin America: geographic structure, phenotypic diversity and self-perception of ancestry based on 7,342 individuals. PLoS Genet. *10*, e1004572.
14. Harvey, S.P. (2016). Ideas of race in early America. Oxford Res. Encycl. https://oxfordre.com/americanhistory/view/10.1093/acrefore/9780199329175.001.0001/acrefore-9780199329175-e-262.
15. Zavala, S. (1968). Los Esclavos Indios en Nueva España (El Colegio de México).
16. Schroeder, H., Ávila-Arcos, M.C., Malaspinas, A.-S., Poznik, G.D., Sandoval-Velasco, M., Carpenter, M.L., Moreno-Mayar, J.V., Sikora, M., Johnson, P.L.F., Allentoft, M.E., et al. (2015). Genome-wide ancestry of 17th-century enslaved Africans from the Caribbean. Proc. Natl. Acad. Sci. USA *112*, 3669–3673.
17. Bourne, J.K., Jr. (2018). Digging for the life stories of long-forgotten slaves. Natl. Geogr. Mag. https://www.nationalgeographic.com/culture/2018/12/charleston-gullah-dna-anson-slave-burials/.
18. Schablitsky, J.M., Witt, K.E., Ramos Madrigal, J., Ellegaard, M.R., Malhi, R.S., and Schroeder, H. (2019). Ancient DNA analysis of a nineteenth century tobacco pipe from a Maryland slave quarter. J. Archaeol. Sci. *105*, 11–18.
19. Fortes-Lima, C., Gessain, A., Ruiz-Linares, A., Bortolini, M.C., Migot-Nabias, F., Bellis, G., Moreno-Mayar, J.V., Restrepo, B.N., Rojas, W., Avendaño-Tamayo, E., et al. (2017). Genome-wide ancestry and demographic history of African-descendant maroon communities from French Guiana and Suriname. Am. J. Hum. Genet. *101*, 725–736.
20. Moreno-Estrada, A., Gravel, S., Zakharia, F., McCauley, J.L., Byrnes, J.K., Gignoux, C.R., Ortiz-Tello, P.A., Martínez, R.J., Hedges, D.J., Morris, R.W., et al. (2013). Reconstructing the population genetic history of the Caribbean. PLoS Genet. *9*, e1003925.
21. Cabrera Torres, J.J., García Martínez, M., and de los, Á. (1998). Utilización, modificación y reúso de los espacios del edificio sede del Hospital Real de San José de los Naturales. PhD thesis (Escuela Nacional de Antropología e Historia).
22. Zedillo, A. (1984). Historia de un Hospital: El Hospital Real de Naturales, First Edition (Editorial del Instituto Mexicano del Seguro Social).
23. López Wario, L.A., Meza Peñaloza, A., and Báez-Molgado, S. (1996). Una muerte violenta en el virreinato (el caso del esqueleto 150 de la línea 8 del Metro, México, D.F.). Rev. la Coord. Nac. Arqueol. del Inst. Nac. Antropol. e Hist. *Ene-jun*, 111–114.
24. Del Castillo Chávez, O. (2000). Condiciones de vida y salud de una muestra poblacional de la Ciudad de México en la época colonial. PhD thesis (Escuela Nacional de Antropología e Historia).
25. Lagunas Rodríguez, Z., and Karam Tapia, C.E. (2003). Cráneos africanos de la época colonial con mutilación dentaria, procedentes del ex Hospital Real de San José de los Naturales de la Ciudad de México, D.F. Estud. Antropol. Biologica (Santiago) *11*, 967–981.
26. Hernández López, P.E., and Negrete Gutiérrez, S.S. (2012). ¿Realmente eran indios? Afinidad biológica entre las personas atendidas en el Hospital Real San José de los Naturales, siglos XVI-XVIII. PhD thesis (Escuela Nacional de Antropología e Historia).
27. Meza, A. (2013). Presencia africana en el cementerio del Hospital Real de San José de los Naturales. Arqueol. Mex. *21*, 40–44.

28. Báez Molgado, S., and Meza-Peñaloza, A. (1995). Análisis de los Restos Óseos del Hospital Real de San José de los Naturales (Individuos Completos). Report. Archivo Técnico de la Dirección de Salvamento Arqueológico (DSA), Instituto Nacional de Antropología e Historia (INAH).

29. Lander, E.S., Linton, L.M., Birren, B., Nusbaum, C., Zody, M.C., Baldwin, J., Devon, K., Dewar, K., Doyle, M., FitzHugh, W., et al.; International Human Genome Sequencing Consortium (2001). Initial sequencing and analysis of the human genome. Nature *409*, 860–921.

30. Patterson, N., Moorjani, P., Luo, Y., Mallick, S., Rohland, N., Zhan, Y., Genschoreck, T., Webster, T., and Reich, D. (2012). Ancient admixture in human history. Genetics *192*, 1065–1093.

31. Fu, Q., Posth, C., Hajdinjak, M., Petr, M., Mallick, S., Fernandes, D., Furtwängler, A., Haak, W., Meyer, M., Mittnik, A., et al. (2016). The genetic history of Ice Age Europe. Nature *534*, 200–205.

32. Korneliussen, T.S., Albrechtsen, A., and Nielsen, R. (2014). ANGSD: analysis of next generation sequencing data. BMC Bioinformatics *15*, 356.

33. Renaud, G., Slon, V., Duggan, A.T., and Kelso, J. (2015). Schmutzi: estimation of contamination and endogenous mitochondrial consensus calling for ancient DNA. Genome Biol. *16*, 224.

34. Wright, L.E., and Schwarcz, H.P. (1998). Stable carbon and oxygen isotopes in human tooth enamel: identifying breastfeeding and weaning in prehistory. Am. J. Phys. Anthropol. *106*, 1–18.

35. Sealy, J.C., van der Merwe, N.J., Thorp, J.A.L., and Lanham, J.L. (1987). Nitrogen isotopic ecology in southern Africa: implications for environmental and dietary tracing. Geochim. Cosmochim. Acta *51*, 2707–2717.

36. Loftus, E., Roberts, P., and Lee-Thorp, J.A. (2016). An isotopic generation: four decades of stable isotope analysis in African archaeology. Azania *51*, 88–114.

37. Walker, P.L., Bathurst, R.R., Richman, R., Gjerdrum, T., and Andrushko, V.A. (2009). The causes of porotic hyperostosis and cribra orbitalia: a reappraisal of the iron-deficiency-anemia hypothesis. Am. J. Phys. Anthropol. *139*, 109–125.

38. Goodman, A.H. (1994). Cartesian reductionism and vulgar adaptationism: issues in the interpretation of nutritional status in prehistory. In Paleonutrition: The Diet of Prehistoric Americans, K. Sobolik, ed. (Southern Illinois University), pp. 163–177.

39. Larsen, C.S. (1997). Bioarchaeology: Interpreting Behavior from the Human Skeleton (Cambridge University).

40. Klaus, H.D., and Tam, M.E. (2009). Contact in the Andes: bioarchaeology of systemic stress in colonial Mórrope, Peru. Am. J. Phys. Anthropol. *138*, 356–368.

41. Wasterlain, S.N., Neves, M.J., and Ferreira, M.T. (2016). Dental modifications in a skeletal sample of enslaved Africans found at Lagos (Portugal). Int. J. Osteoarchaeol. *26*, 621–632.

42. Alves, R.V., Garcia, S.J., Marques, A., and Wasterlain, S.N. (2016). Osteological analysis of a skeleton with intentional dental modifications, exhumed from Largo do Carmo (17th – 18th centuries), Lisbon. Antropol. Port. *32*, 61–75.

43. Lignitz, H. (1919). Die künstlichen Zahnverstümmlungen in Afrika im Lichte der Kulturkreisforschung. Anthropos *14/15*, 891–943.

44. Rosa, A., and Brehem, A. (2011). African human mtDNA phylogeography at-a-glance. J. Anthropol. Sci. *89*, 25–58.

45. Brehm, A., Pereira, L., Bandelt, H.J., Prata, M.J., and Amorim, A. (2002). Mitochondrial portrait of the Cabo Verde archipelago: the Senegambian outpost of Atlantic slave trade. Ann. Hum. Genet. *66*, 49–60.

46. González, A.M., Cabrera, V.M., Larruga, J.M., Tounkara, A., Noumsi, G., Thomas, B.N., and Moulds, J.M. (2006). Mitochondrial DNA variation in Mauritania and Mali and their genetic relationship to other Western Africa populations. Ann. Hum. Genet. *70*, 631–657.

47. Pereira, L., Macaulay, V., Torroni, A., Scozzari, R., Prata, M.J., and Amorim, A. (2001). Prehistoric and historic traces in the mtDNA of Mozambique: insights into the Bantu expansions and the slave trade. Ann. Hum. Genet. *65*, 439–458.

48. Salas, A., Richards, M., De la Fe, T., Lareu, M.-V., Sobrino, B., Sánchez-Diz, P., Macaulay, V., and Carracedo, A. (2002). The making of the African mtDNA landscape. Am. J. Hum. Genet. *71*, 1082–1111.

49. Underhill, P.A., Shen, P., Lin, A.A., Jin, L., Passarino, G., Yang, W.H., Kauffman, E., Bonné-Tamir, B., Bertranpetit, J., Francalacci, P., et al. (2000). Y chromosome sequence variation and the history of human populations. Nat. Genet. *26*, 358–361.

50. Vallone, P.M., and Butler, J.M. (2004). Y-SNP typing of U.S. African American and Caucasian samples using allele-specific hybridization and primer extension. J. Forensic Sci. *49*, 723–732.

51. Schuster, S.C., Miller, W., Ratan, A., Tomsho, L.P., Giardine, B., Kasson, L.R., Harris, R.S., Petersen, D.C., Zhao, F., Qi, J., et al. (2010). Complete Khoisan and Bantu genomes from southern Africa. Nature *463*, 943–947.

52. Trombetta, B., Cruciani, F., Sellitto, D., and Scozzari, R. (2011). A new topology of the human Y chromosome haplogroup E1b1 (E-P2) revealed through the use of newly characterized binary polymorphisms. PLoS ONE *6*, e16073.

53. Martínez-Cortés, G., Salazar-Flores, J., Haro-Guerrero, J., Rubi-Castellanos, R., Velarde-Félix, J.S., Muñoz-Valle, J.F., López-Casamichana, M., Carrillo-Tapia, E., Canseco-Avila, L.M., Bravi, C.M., et al. (2013). Maternal admixture and population structure in Mexican-Mestizos based on mtDNA haplogroups. Am. J. Phys. Anthropol. *151*, 526–537.

54. Szolek, A., Schubert, B., Mohr, C., Sturm, M., Feldhahn, M., and Kohlbacher, O. (2014). OptiType: precision HLA typing from next-generation sequencing data. Bioinformatics *30*, 3310–3316.

55. Assane, A.A.A., Fabricio-Silva, G.M., Cardoso-Oliveira, J., Mabunda, N.E.J., Sousa, A.M., Jani, I.V., Ferreira, O.C., Jr., and Porto, L.C.M.S. (2010). Human leukocyte antigen-A, -B, and -DRB1 allele and haplotype frequencies in the Mozambican population: a blood donor-based population study. Hum. Immunol. *71*, 1027–1032.

56. Paximadis, M., Mathebula, T.Y., Gentle, N.L., Vardas, E., Colvin, M., Gray, C.M., Tiemessen, C.T., and Puren, A. (2012). Human leukocyte antigen class I (A, B, C) and II (DRB1) diversity in the black and Caucasian South African population. Hum. Immunol. *73*, 80–92.

57. Arlehamn, C.S.L., Copin, R., Leary, S., Mack, S.J., Phillips, E., Mallal, S., Sette, A., Blatner, G., Siefers, H., and Ernst, J.D.; TBRU-ASTRa Study Team (2017). Sequence-based HLA-A, B, C, DP, DQ, and DR typing of 100 Luo infants from the Boro area of Nyanza Province, Kenya. Hum. Immunol. *78*, 325–326.

58. Grifoni, A., Sidney, J., Carpenter, C., Phillips, E., Mallal, S., Scriba, T.J., Sette, A., and Lindestam Arlehamn, C.S. (2018). Sequence-based HLA-A, B, C, DP, DQ, and DR typing of 159 individuals from the Worcester region of the Western Cape province of South Africa. Hum. Immunol. *79*, 143–144.

59. Maiers, M., Gragert, L., and Klitz, W. (2007). High-resolution HLA alleles and haplotypes in the United States population. Hum. Immunol. *68*, 779–788.

60. Nunes, K., Piovezan, B., Torres, M.A., Pontes, G.N., Kimura, L., Carnavalli, J.E.P., Mingroni Netto, R.C., Moraes, M.E., and Meyer, D. (2016). Population variation of HLA genes in rural communities in Brazil, the Quilombos from the Vale do Ribeira, São Paulo - Brazil. Hum. Immunol. *77*, 447–448.

61. Tang, J., Naik, E., Costello, C., Karita, E., Rivers, C., Allen, S., and Kaslow, R.A. (2000). Characteristics of HLA class I and class II polymorphisms in Rwandan women. Exp. Clin. Immunogenet. *17*, 185–198.

62. Fu, Q., Li, H., Moorjani, P., Jay, F., Slepchenko, S.M., Bondarev, A.A., Johnson, P.L.F., Aximu-Petri, A., Prüfer, K., de Filippo, C., et al. (2014). Genome sequence of a 45,000-year-old modern human from western Siberia. Nature *514*, 445–449.

63. Price, T.D., Tiesler, V., and Burton, J.H. (2006). Early African Diaspora in colonial Campeche, Mexico: strontium isotopic evidence. Am. J. Phys. Anthropol. *130*, 485–490.

64. Price, T.D., Burton, J.H., Cucina, A., Zabala, P., Frei, R., Tykot, R.H., and Tiesler, V. (2012). Isotopic studies of human skeletal remains from a sixteenth to seventeenth century AD churchyard in Campeche, Mexico. Curr. Anthropol. *53*, 396–433.

65. Hodell, D.A., Quinn, R.L., Brenner, M., and Kamenov, G. (2004). Spatial variation of strontium isotopes ($^{87}Sr/^{86}Sr$) in the Maya region: a tool for tracking ancient human migration. J. Archaeol. Sci. *31*, 585–601.

66. Juarez, C.A. (2008). Strontium and geolocation, the pathway to identification for deceased undocumented mexican border-crossers: a preliminary report. J. Forensic Sci. *53*, 46–49.

67. Schroeder, H., O'Connell, T.C., Evans, J.A., Shuler, K.A., and Hedges, R.E.M. (2009). Trans-Atlantic slavery: isotopic evidence for forced migration to Barbados. Am. J. Phys. Anthropol. *139*, 547–557.

68. Hübler, R., Key, F.M., Warinner, C., Bos, K.I., Krause, J., and Herbig, A. (2019). HOPS: automated detection and authentication of pathogen DNA in archaeological remains. Genome Biol. *20*, 280.

69. Kramvis, A. (2014). Genotypes and genetic variability of hepatitis B virus. Intervirology *57*, 141–150.

70. Pourkarim, M.R., Amini-Bavil-Olyaee, S., Kurbanov, F., Van Ranst, M., and Tacke, F. (2014). Molecular identification of hepatitis B virus genotypes/subgenotypes: revised classification hurdles and updated resolutions. World J. Gastroenterol. *20*, 7152–7168.

71. Schuenemann, V.J., Kumar Lankapalli, A., Barquera, R., Nelson, E.A., Iraíz Hernández, D., Acuña Alonzo, V., Bos, K.I.K.I., Márquez Morfín, L., Herbig, A., and Krause, J. (2018). Historic Treponema pallidum genomes from Colonial Mexico retrieved from archaeological remains. PLoS Negl. Trop. Dis. *12*, e0006447.

72. Hurston, Z.N. (2018). Barracoon. The Story of the Last "Black Cargo,", First Edition (Amistad Press/HarperCollins Publishers).

73. Corona Paredes, O. (2004). Informe Final del Rescate Arqueológico en el ex Templo de Corpus Christi. Report. Dirección de Salvamento Arqueológico (INAH).

74. Green, L.D., Derr, J.N., and Knight, A. (2000). mtDNA affinities of the peoples of North-Central Mexico. Am. J. Hum. Genet. *66*, 989–998.

75. Guardado-Estrada, M., Juarez-Torres, E., Medina-Martinez, I., Wegier, A., Macías, A., Gomez, G., Cruz-Talonia, F., Roman-Bassaure, E., Piñero, D., Kofman-Alfaro, S., and Berumen, J. (2009). A great diversity of Amerindian mitochondrial DNA ancestry is present in the Mexican mestizo population. J. Hum. Genet. *54*, 695–705.

76. Barquera, R., Hernandez-Zaragoza, D.I., and Bravo Acevedo, A. (2018). The immunogenetic diversity of the HLA system in Mexico correlates with underlying population genetic structure. The Allele Frequency Net Database. http://allelefrequencies.net/hla6006a.asp?page=1&hla_locus=&hla_locus_type=Classical&hla_allele1=&hla_allele2=&hla_selection=&hla_pop_selection=&hla_population=&hla_country=Mexico&hla_dataset=&hla_region=&hla_ethnic=&hla_study=Other&hla_sample_size=&hla_s.

77. Li, Z.-K., Nie, J.-J., Li, J., and Zhuang, H. (2013). The effect of HLA on immunological response to hepatitis B vaccine in healthy people: a meta-analysis. Vaccine *31*, 4355–4361.

78. Yoon, J.H., Shin, S., In, Jw., Chang, J.Y., Song, E.Y., and Roh, E.Y. (2014). Association of HLA alleles with the responsiveness to hepatitis B virus vaccination in Korean infants. Vaccine *32*, 5638–5644.

79. Nishida, N., Sawai, H., Kashiwase, K., Minami, M., Sugiyama, M., Seto, W.-K., Yuen, M.-F., Posuwan, N., Poovorawan, Y., Ahn, S.H., et al. (2014). New susceptibility and resistance HLA-DP alleles to HBV-related diseases identified by a trans-ethnic association study in Asia. PLoS ONE *9*, e86449.

80. Jiang, H.-W., Tian, H.-Q., Liu, H., Li, N., Zhao, Y., and Zhang, F.-R. (2011). Association of the HLA-DRB1 locus with syphilis in a Chinese population. Int. J. Infect. Dis. *15*, e342–e345.

81. Aguirre Beltrán, G. (1944). The slave trade in Mexico. Hisp. Am. Hist. Rev. *24*, 412–431.

82. Lavanchy, D., and Kane, M. (2016). Global epidemiology of hepatitis B virus infection BT - hepatitis B virus in human diseases. In Hepatitis B Virus in Human Diseases, Y.-F. Liaw, and F. Zoulim, eds. (Springer International Publishing), pp. 187–203.

83. Krause-Kyora, B., Susat, J., Key, F.M., Kühnert, D., Bosse, E., Immel, A., Rinne, C., Kornell, S.-C., Yepes, D., Franzenburg, S., et al. (2018). Neolithic and medieval virus genomes reveal complex evolution of hepatitis B. eLife *7*, e36666.

84. Mühlemann, B., Jones, T.C., Damgaard, P.B., Allentoft, M.E., Shevnina, I., Logvin, A., Usmanova, E., Panyushkina, I.P., Boldgiv, B., Bazartseren, T., et al. (2018). Ancient hepatitis B viruses from the Bronze Age to the Medieval period. Nature *557*, 418–423.

85. Andernach, I.E., Nolte, C., Pape, J.W., and Muller, C.P. (2009). Slave trade and hepatitis B virus genotypes and subgenotypes in Haiti and Africa. Emerg. Infect. Dis. *15*, 1222–1228.

86. Morfín, M., and Espinoza, L.H.P. (2006). Salud y Sociedad en el México Prehispánico y Colonial (Instituto Nacional de Antropología e Historia/Escuela Nacional de Antropología e Historia).

87. Márquez Morfín, L., and Meza Manzanilla, M. (2015). Sífilis en la Ciudad de México: análisis osteopatológico. Cuicuilco *22*, 89–126.

88. Schubert, M., Lindgreen, S., and Orlando, L. (2016). AdapterRemoval v2: rapid adapter trimming, identification, and read merging. BMC Res. Notes *9*, 88.

89. Li, H., and Durbin, R. (2010). Fast and accurate long-read alignment with Burrows-Wheeler transform. Bioinformatics *26*, 589–595.

90. Peltzer, A., Jäger, G., Herbig, A., Seitz, A., Kniep, C., Krause, J., and Nieselt, K. (2016). EAGER: efficient ancient genome reconstruction. Genome Biol. *17*, 60.

91. Kearse, M., Moir, R., Wilson, A., Stones-Havas, S., Cheung, M., Sturrock, S., Buxton, S., Cooper, A., Markowitz, S., Duran, C., et al. (2012). Geneious Basic: an integrated and extendable desktop software platform for the organization and analysis of sequence data. Bioinformatics *28*, 1647–1649.

92. Jónsson, H., Ginolhac, A., Schubert, M., Johnson, P.L.F., and Orlando, L. (2013). mapDamage2.0: fast approximate Bayesian estimates of ancient DNA damage parameters. Bioinformatics *29*, 1682–1684.

93. Skoglund, P., Northoff, B.H., Shunkov, M.V., Derevianko, A.P., Pääbo, S., Krause, J., and Jakobsson, M. (2014). Separating endogenous ancient DNA from modern day contamination in a Siberian Neandertal. Proc. Natl. Acad. Sci. USA *111*, 2229–2234.

94. Li, H., Handsaker, B., Wysoker, A., Fennell, T., Ruan, J., Homer, N., Marth, G., Abecasis, G., and Durbin, R.; 1000 Genome Project Data Processing Subgroup (2009). The Sequence Alignment/Map format and SAMtools. Bioinformatics *25*, 2078–2079.

95. Li, H. (2011). A statistical framework for SNP calling, mutation discovery, association mapping and population genetical parameter estimation from sequencing data. Bioinformatics *27*, 2987–2993.

96. Patterson, N., Price, A.L., and Reich, D. (2006). Population structure and eigenanalysis. PLoS Genet. *2*, e190.

97. Venegas Ramírez, C. (1973). Régimen Hospitalario para Indios en la Nueva España (Secretaría de Educación Pública/Instituto Nacional de Antropología e Historia).

98. Suárez, M. (1988). Hospitales y sociedad en la Ciudad de México en el siglo XVI. PhD thesis (Universidad Autónoma Metropolitana-Azcapotzalco).

99. Muriel, J. (1990). Hospital Real de Sanct Joseph de los Naturales, México, D. F. In Hospitales de la Nueva España. T. 1. Fundaciones del siglo XVI (Universidad Nacional Autónoma de México—Instituto de Investigaciones Históricas/Cruz Roja Mexicana), pp. 127–148.

100. McCaa, R. (1995). Spanish and Nahuatl views on smallpox and demographic catastrophe in Mexico. J. Interdiscip. Hist. *25*, 397–431.

101. Ruíz Albarrán, P., and del, C. (2012). Estudios de variabilidad biológica en la colección esquelética Hospital Real de Naturales. Un acercamiento a

través de la técnica de Morfometría Geométrica. PhD thesis (Escuela Nacional de Antropología e Historia).

102. Fierros Millán, J. (2009). El Hospital Real de Naturales (1701-1741), un hospital disputado de la capital novohispana. PhD thesis (Escuela Nacional de Antropología e Historia).
103. Garve, M. (2011). Rituelle Deformierungen der Zähne und deren Einfluss auf das orofaziale System bei Naturvölkern am Beispiel der Bench in Südwest- Äthiopien. PhD thesis (Universitätsmedizin der Ernst-Moritz-Arndt-Universität Greifswald).
104. Goodman, A.H., and Martin, D.L. (2002). Reconstructing health profiles from skeletal remains. In The Backbone of History. Health and Nutricion of the Western Hemisphere, R.H. Steckel, and J.C. Rose, eds. (Cambridge University), pp. 11–60.
105. Ortner, D.J. (2003). Identification of Pathological Conditions in Human Skeletal Remains, Second Edition (Academic).
106. Buikstra, J.E., and Ubelaker, D.H. (1994). Standards for Data Collection from Human Skeletal Remains: Proceedings of a Seminar at the Field Museum of Natural History (Arkansas Archeological Survey).
107. Hernández Espinoza, P.O., and Rodríguez Lagunas, Z. (2015). Manual de Osteología, Third Edition (Instituto Nacional de Antropología e Historia/ Escuela Nacional de Antropología e Historia).
108. Reichart, P.A., Creutz, U., and Scheifele, C. (2008). Dental mutilations and associated alveolar bone pathology in African skulls of the anthropological skull collection, Charité, Berlin. J. Oral Pathol. Med. *37*, 50–55.
109. Hefner, J.T. (2009). Cranial nonmetric variation and estimating ancestry. J. Forensic Sci. *54*, 985–995.
110. Coelho, J. d'Oliveira, and Navega, D. (2011). Cranial nonmetric traits ancestry estimation. Osteomics. http://osteomics.com/hefneR/.
111. Villegas Camposeco, B., and del, C. (2018). ¿Tu origen, es mi origen? Frecuencia y variación de rasgos no-métricos craneales en población mexicana contemporánea. PhD thesis (Escuela Nacional de Antropología e Historia).
112. Bruzek, J. (2002). A method for visual determination of sex, using the human hip bone. Am. J. Phys. Anthropol. *117*, 157–168.
113. DiGangi, E.A., Bethard, J.D., Kimmerle, E.H., and Konigsberg, L.W. (2009). A new method for estimating age-at-death from the first rib. Am. J. Phys. Anthropol. *138*, 164–176.
114. McKern, T.W., and Stewart, T.D. (1957). Skeletal Age Changes in Young American Males: Analysed from the Standpoint of Age Identification (Headquarters, Quartermaster Research & Development Command, Quartermaster Research & Development Center, Environmental Protection Research Division).
115. Lovejoy, C.O., Meindl, R.S., Pryzbeck, T.R., and Mensforth, R.P. (1985). Chronological metamorphosis of the auricular surface of the ilium: a new method for the determination of adult skeletal age at death. Am. J. Phys. Anthropol. *68*, 15–28.
116. Henríquez, M., and Arriaza, B. (2013). Distribución y frecuencia de nódulos de Schmörl en la columna vertebral de poblaciones prehispánicas de Arica: ¿Indicadores de la carga laboral? Rev. Antropol. Chil. *45*, 311–319.
117. Phenice, T.W. (1969). A newly developed visual method of sexing the os pubis. Am. J. Phys. Anthropol. *30*, 297–301.
118. Ubelaker, D.H. (1991). Perimortem and postmortem modifications of human bone: lessons from forensic anthropology. Anthropologie *29*, 171–174.
119. Ascough, P.L., Cook, G.T., and Dugmore, A. (2005). Methodological approaches to determining the marine radiocarbon reservoir effect. Prog. Phys. Geogr. *29*, 532–547.
120. Bronk Ramsey, C. (2008). Radiocarbon dating: revolutions in understanding. Archaeometry *50*, 249–275.
121. AlQahtani, S.J., Hector, M.P., and Liversidge, H.M. (2010). Brief communication: the London atlas of human tooth development and eruption. Am. J. Phys. Anthropol. *142*, 481–490.
122. Logan, W.H.G., and Kronfeld, R. (1933). Development of the human jaws and surrounding structures from birth to the age of fifteen years. J. Am. Dent. Assoc. *20*, 379–428.
123. Richards, M.P., and Hedges, R.E.M. (1999). Stable isotope evidence for similarities in the types of marine foods used by late Mesolithic humans at sites along the Atlantic coast of Europe. J. Archaeol. Sci. *26*, 717–722.
124. van Klinken, G.J. (1999). Bone collagen quality indicators for palaeodietary and radiocarbon measurements. J. Archaeol. Sci. *26*, 687–695.
125. DeNiro, M.J. (1985). Postmortem preservation and alteration of *in vivo* bone collagen isotope ratios in relation to palaeodietary reconstruction. Nature *317*, 806–809.
126. Roberts, P., Fernandes, R., Craig, O.E., Larsen, T., Lucquin, A., Swift, J., and Zech, J. (2018). Calling all archaeologists: guidelines for terminology, methodology, data handling, and reporting when undertaking and reviewing stable isotope applications in archaeology. Rapid Commun. Mass Spectrom. *32*, 361–372.
127. Ambrose, S.H., and Norr, L. (1993). Experimental evidence for the relationship of the carbon isotope ratios of whole diet and dietary protein to those of bone collagen and carbonate. In Prehistoric Human Bone: Archaeology at the Molecular Level, J.B. Lambert, and G. Grupe, eds. (Springer Berlin Heidelberg), pp. 1–37.
128. Smith, B.N., and Epstein, S. (1971). Two categories of c/c ratios for higher plants. Plant Physiol. *47*, 380–384.
129. Farquhar, G.D., Ehleringer, J.R., and Hubick, K.T. (1989). Carbon isotope discrimination and photosynthesis. Annu. Rev. Plant Physiol. Plant Mol. Biol. *40*, 503–537.
130. Tieszen, L.L. (1991). Natural variations in the carbon isotope values of plants: implications for archaeology, ecology, and paleoecology. J. Archaeol. Sci. *18*, 227–248.
131. Deniro, M.J., and Epstein, S. (1981). Influence of diet on the distribution of nitrogen isotopes in animals. Geochim. Cosmochim. Acta *45*, 341–351.
132. Ambrose, S.H. (1991). Effects of diet, climate and physiology on nitrogen isotope abundances in terrestrial foodwebs. J. Archaeol. Sci. *18*, 293–317.
133. Hedges, R.E.M., and Reynard, L.M. (2007). Nitrogen isotopes and the trophic level of humans in archaeology. J. Archaeol. Sci. *34*, 1240–1251.
134. Schoeninger, M.J., and DeNiro, M.J. (1984). Nitrogen and carbon isotopic composition of bone collagen from marine and terrestrial animals. Geochim. Cosmochim. Acta *48*, 625–639.
135. Dufour, E., Bocherens, H., and Mariotti, A. (1999). Palaeodietary implications of isotopic variability in Eurasian lacustrine fish. J. Archaeol. Sci. *26*, 617–627.
136. Handler, J.S. (2002). Survivors of the middle passage: life histories of enslaved Africans in British America. Slavery Abol. *23*, 25–56.
137. Cox, G., Sealy, J., Schrire, C., and Morris, A. (2001). Stable carbon and nitrogen isotopic analyses of the underclass at the colonial Cape of Good Hope in the eighteenth and nineteenth centuries. World Archaeol. *33*, 73–97.
138. Carney, J.A. (2001). African rice in the Columbian exchange. J. Afr. Hist. *42*, 377–396.
139. Stahl, A.B. (1999). The archaeology of global encounters viewed from Banda, Ghana. Afr. Archaeol. Rev. *16*, 5–81.
140. Bastos, M.Q.R., Santos, R.V., de Souza, S.M.F.M., Rodrigues-Carvalho, C., Tykot, R.H., Cook, D.C., and Santos, R.V. (2016). Isotopic study of geographic origins and diet of enslaved Africans buried in two Brazilian cemeteries. J. Archaeol. Sci. *70*, 82–90.
141. Laffoon, J.E., Espersen, R., and Mickleburgh, H.L. (2018). The life history of an enslaved African: multiple isotope evidence for forced childhood migration from Africa to the Caribbean and associated dietary change. Archaeometry *60*, 350–365.
142. Fernandes, R., Rinne, C., Nadeau, M.-J., and Grootes, P. (2016). Towards the use of radiocarbon as a dietary proxy: establishing a first wide-ranging radiocarbon reservoir effects baseline for Germany. Environ. Archaeol. *21*, 285–294.

143. Cook, G.T., and van der Plicht, J. (2006). Radiocarbon dating: conventional method. In Encyclopedia of Quaternary Science, S. Elias, ed. (Elsevier), pp. 2899–2911.

144. Keaveney, E.M., and Reimer, P.J. (2012). Understanding the variability in freshwater radiocarbon reservoir offsets: a cautionary tale. J. Archaeol. Sci. *39*, 1306–1316.

145. Jull, A.J.T., Burr, G.S., and Hodgins, G.W.L. (2013). Radiocarbon dating, reservoir effects, and calibration. Quat. Int. *299*, 64–71.

146. Rohland, N., and Hofreiter, M. (2007). Ancient DNA extraction from bones and teeth. Nat. Protoc. *2*, 1756–1762.

147. Dabney, J., Knapp, M., Glocke, I., Gansauge, M.-T., Weihmann, A., Nickel, B., Valdiosera, C., García, N., Pääbo, S., Arsuaga, J.-L., and Meyer, M. (2013). Complete mitochondrial genome sequence of a Middle Pleistocene cave bear reconstructed from ultrashort DNA fragments. Proc. Natl. Acad. Sci. USA *110*, 15758–15763.

148. Briggs, A.W., Stenzel, U., Johnson, P.L.F., Green, R.E., Kelso, J., Prüfer, K., Meyer, M., Krause, J., Ronan, M.T., Lachmann, M., and Pääbo, S. (2007). Patterns of damage in genomic DNA sequences from a Neandertal. Proc. Natl. Acad. Sci. USA *104*, 14616–14621.

149. Meyer, M., and Kircher, M. (2010). Illumina sequencing library preparation for highly multiplexed target capture and sequencing. Cold Spring Harb. Protoc. *2010*, pdb.prot5448.

150. Rohland, N., Harney, E., Mallick, S., Nordenfelt, S., and Reich, D. (2015). Partial uracil-DNA-glycosylase treatment for screening of ancient DNA. Philos. Trans. R. Soc. B Biol. Sci. *370*, 20130624.

151. Gnirke, A., Melnikov, A., Maguire, J., Rogov, P., LeProust, E.M., Brockman, W., Fennell, T., Giannoukos, G., Fisher, S., Russ, C., et al. (2009). Solution hybrid selection with ultra-long oligonucleotides for massively parallel targeted sequencing. Nat. Biotechnol. *27*, 182–189.

152. Mathieson, I., Lazaridis, I., Rohland, N., Mallick, S., Patterson, N., Roodenberg, S.A., Harney, E., Stewardson, K., Fernandes, D., Novak, M., et al. (2015). Genome-wide patterns of selection in 230 ancient Eurasians. Nature *528*, 499–503.

153. Fu, Q., Meyer, M., Gao, X., Stenzel, U., Burbano, H.A., Kelso, J., and Pääbo, S. (2013). DNA analysis of an early modern human from Tianyuan Cave, China. Proc. Natl. Acad. Sci. USA *110*, 2223–2227.

154. Fu, Q., Hajdinjak, M., Moldovan, O.T., Constantin, S., Mallick, S., Skoglund, P., Patterson, N., Rohland, N., Lazaridis, I., Nickel, B., et al. (2015). An early modern human from Romania with a recent Neanderthal ancestor. Nature *524*, 216–219.

155. Ghodsi, M., Liu, B., and Pop, M. (2011). DNACLUST: accurate and efficient clustering of phylogenetic marker genes. BMC Bioinformatics *12*, 271.

156. Immel, A., Key, F.M., Szolek, A., Barquera, R., Robinson, M.K., Spyrou, M.A., Susat, J., Krause-Kyora, B., Bos, K.I., Forrest, S., et al. (2019). Genomic DNA from Late Medieval plague victims suggests effect of Yersinia pestis on human immunity genes. bioRxiv.

157. O'Leary, N.A., Wright, M.W., Brister, J.R., Ciufo, S., Haddad, D., McVeigh, R., Rajput, B., Robbertse, B., Smith-White, B., Ako-Adjei, D., et al. (2016). Reference sequence (RefSeq) database at NCBI: current status, taxonomic expansion, and functional annotation. Nucleic Acids Res. *44* (D1), D733–D745.

158. Robinson, J., Halliwell, J.A., Hayhurst, J.D., Flicek, P., Parham, P., and Marsh, S.G.E. (2015). The IPD and IMGT/HLA database: allele variant databases. Nucleic Acids Res. *43*, D423–D431.

159. Holdsworth, R., Hurley, C.K., Marsh, S.G.E., Lau, M., Noreen, H.J., Kempenich, J.H., Setterholm, M., and Maiers, M. (2009). The HLA dictionary 2008: a summary of HLA-A, -B, -C, -DRB1/3/4/5, and -DQB1 alleles and their association with serologically defined HLA-A, -B, -C, -DR, and -DQ antigens. Tissue Antigens *73*, 95–170.

160. Weese, D., Holtgrewe, M., and Reinert, K. (2012). RazerS 3: faster, fully sensitive read mapping. Bioinformatics *28*, 2592–2599.

161. Schiffels, S. (2018). sequenceTools. https://github.com/stschiff/sequenceTools.git.

162. Andrews, R.M., Kubacka, I., Chinnery, P.F., Lightowlers, R.N., Turnbull, D.M., and Howell, N. (1999). Reanalysis and revision of the Cambridge reference sequence for human mitochondrial DNA. Nat. Genet. *23*, 147.

163. Weissensteiner, H., Pacher, D., Kloss-Brandstätter, A., Forer, L., Specht, G., Bandelt, H.-J.J., Kronenberg, F., Salas, A., and Schönherr, S. (2016). HaploGrep 2: mitochondrial haplogroup classification in the era of high-throughput sequencing. Nucleic Acids Res. *44* (W1), W58–W63.

164. Vianello, D., Sevini, F., Castellani, G., Lomartire, L., Capri, M., and Franceschi, C. (2013). HAPLOFIND: a new method for high-throughput mtDNA haplogroup assignment. Hum. Mutat. *34*, 1189–1194.

165. Katoh, K., and Standley, D.M. (2013). MAFFT multiple sequence alignment software version 7: improvements in performance and usability. Mol. Biol. Evol. *30*, 772–780.

166. Paradis, E. (2010). pegas: an R package for population genetics with an integrated-modular approach. Bioinformatics *26*, 419–420.

167. Banks, R. (2018). International Society of Genetic Genealogy database (ISOGG) Y-DNA. Y-DNA Haplogr. Tree 2018 Version 13.174. https://isogg.org/tree/.

168. Bryc, K., Velez, C., Karafet, T., Moreno-Estrada, A., Reynolds, A., Auton, A., Hammer, M., Bustamante, C.D., and Ostrer, H. (2010). Colloquium paper: genome-wide patterns of population structure and admixture among Hispanic/Latino populations. Proc. Natl. Acad. Sci. USA *107* (*Suppl 2*), 8954–8961.

169. Alexander, D.H., Novembre, J., and Lange, K. (2009). Fast model-based estimation of ancestry in unrelated individuals. Genome Res. *19*, 1655–1664.

170. Alexander, D.H., Novembre, J., and Lange, K. (2016). ADMIXTURE. https://www.genetics.ucla.edu/software/admixture/download.html.

171. Moreno-Estrada, A., Gignoux, C.R., Fernández-López, J.C., Zakharia, F., Sikora, M., Contreras, A.V., Acuña-Alonzo, V., Sandoval, K., Eng, C., Romero-Hidalgo, S., et al. (2014). Human genetics. The genetics of Mexico recapitulates Native American substructure and affects biomedical traits. Science *344*, 1280–1285.

172. Patterson, N. (2012). DReichLab/AdmixTools. https://github.com/DReichLab/AdmixTools.

173. Castresana, J. (2000). Selection of conserved blocks from multiple alignments for their use in phylogenetic analysis. Mol. Biol. Evol. *17*, 540–552.

174. Stamatakis, A. (2014). RAxML version 8: a tool for phylogenetic analysis and post-analysis of large phylogenies. Bioinformatics *30*, 1312–1313.

175. Herbig, A., Maixner, F., Bos, K.I., Zink, A., Krause, J., and Huson, D.H. (2016). MALT: fast alignment and analysis of metagenomic DNA sequence data applied to the Tyrolean Iceman. bioRxiv. https://doi.org/10.1101/050559.

176. Broad Institute (2019). Picard Toolkit (GitHub Repos).

177. Bos, K.I., Harkins, K.M., Herbig, A., Coscolla, M., Weber, N., Comas, I., Forrest, S.A., Bryant, J.M., Harris, S.R., Schuenemann, V.J., et al. (2014). Pre-Columbian mycobacterial genomes reveal seals as a source of New World human tuberculosis. Nature *514*, 494–497.

178. Didelot, X., and Wilson, D.J. (2015). ClonalFrameML: efficient inference of recombination in whole bacterial genomes. PLoS Comput. Biol. *11*, e1004041.

STAR★METHODS

KEY RESOURCES TABLE

REAGENT or RESOURCE	SOURCE	IDENTIFIER
Biological Samples		
Ancient individual	This study/ San José de los Naturales archaeological site	SJN001/ *ML8 SL 150*
Ancient individual	This study/ San José de los Naturales archaeological site	SJN002/ *ML8 San José 214*
Ancient individual	This study/ San José de los Naturales archaeological site	SJN003/ *ML8 SLU9B 296*
Chemicals, Peptides, and Recombinant Proteins		
2x HI-RPM hybridization buffer	Agilent Technologies	Cat# 5190-0403
Herculase II Fusion DNA Polymerase	Agilent Technologies	Cat# 600679
Pfu Turbo Cx Hotstart DNA Polymerase	Agilent Technologies	Cat# 600412
D1000 ScreenTapes	Agilent Technologies	Cat# 5067-5582
D1000 Reagents	Agilent Technologies	Cat# 5067-5583
0.5 M EDTA pH 8.0	BioExpress	Cat# E177
Sera-Mag Magnetic Speed-beads Carboxylate-Modified (1 mm, 3EDAC/PA5)	GE LifeScience	Cat# 65152105050250
Bst DNA Polymerase2.0, large frag.	New England Biolabs	Cat# M0537
UGI	New England Biolabs	Cat# M0281
USER enzyme	New England Biolabs	Cat# M5505
PE buffer concentrate	QiaGEN	Cat# 19065
1 M Tris-HCl pH 8.0	Sigma Aldrich	Cat# AM9856
1M NaOH	Sigma Aldrich	Cat# 71463
20% SDS	Sigma Aldrich	Cat# 5030
3M Sodium Acetate (pH 5.2)	Sigma Aldrich	Cat# S7899
5M NaCl	Sigma Aldrich	Cat# S5150
Ethanol	Sigma Aldrich	Cat# E7023
Guanidine hydrochloride	Sigma Aldrich	Cat# G3272
Isopropanol	Sigma Aldrich	Cat# 650447
PEG-8000	Sigma Aldrich	Cat# 89510
Proteinase K	Sigma Aldrich	Cat# P6556
Tween-20	Sigma Aldrich	Cat# P9416
Water	Sigma Aldrich	Cat# W4502
10x Buffer Tango	Thermo Fisher Scientific	Cat# BY5
50x Denhardt's solution	Thermo Fisher Scientific	Cat# 750018
ATP	Thermo Fisher Scientific	Cat# R0441
dNTP Mix	Thermo Fisher Scientific	Cat# R1121
Dynabeads MyOne Streptavidin T1	Thermo Fisher Scientific	Cat# 65602
DyNAmo HS SYBR Green qPCR Kit	Thermo Fisher Scientific	Cat# F410L
GeneAmp 10x PCR Gold Buffer	Thermo Fisher Scientific	Cat# 4379874
Human Cot-I DNA	Thermo Fisher Scientific	Cat# 15279011
Salmon sperm DNA	Thermo Fisher Scientific	Cat# 15632-011
SSC Buffer (20x)	Thermo Fisher Scientific	Cat# AM9770
T4 DNA Ligase	Thermo Fisher Scientific	Cat# EL0011
T4 DNA Polymerase	Thermo Fisher Scientific	Cat# EP0062
T4 Polynucleotide Kinase	Thermo Fisher Scientific	Cat# EK0032

(*Continued on next page*)

Continued

REAGENT or RESOURCE	SOURCE	IDENTIFIER
Acetone, certified ACS	VWR	Cat# BDH1101-4LP
Dichloromethane, certified ACS	VWR	Cat# EMD-DX0835-3
Hydrochloric acid, 6N, 0.5N & 0.01N	VWR	Cat# EMD-HX0603-3
Critical Commercial Assays		
DyNAmo Flash SYBR Green qPCR Kit	Life Technologies	Cat# F-415L
High Pure Extender from Viral Nucleic Acid Large Volume Kit	Roche	Cat# 5114403001
MinElute PCR Purification Kit	QiaGEN	Cat# 28006
NextSeq 500/550 High Output Kit v2 (150 cycles)	Illumina	Cat# FC-404-2002
HiSeq 4000 SBS Kit (50/75 cycles)	Illumina	Cat# FC-410-1001/2
Deposited Data		
Raw and analyzed data (European Nucleotide Archive)	This study	ENA: PRJEB37490
Software and Algorithms		
AdapterRemoval v2	[88]	https://github.com/MikkelSchubert/adapterremoval
ADMIXTOOLS	[30]	https://github.com/DReichLab/AdmixTools
ANGSD	[32]	https://github.com/ANGSD/angsd
BWA	[89]	http://bio-bwa.sourceforge.net/
Dedup	[90]	https://eager.readthedocs.io/en/latest/
EAGER	[90]	https://eager.readthedocs.io/en/latest/
Geneious R8.1.974	[91]	https://www.geneious.com/
mapDamage2.0	[92]	https://ginolhac.github.io/mapDamage/
OptiType 1.3.1	[54]	https://github.com/FRED-2/OptiType
PMDtools	[93]	https://github.com/pontussk/PMDtools
Samtools	[94, 95]	http://samtools.sourceforge.net/
Schmutzi	[33]	https://grenaud.github.io/schmutzi/
SeqPrep	https://github.com/jstjohn/SeqPrep	https://github.com/jstjohn/SeqPrep
smartpca	[96]	https://www.hsph.harvard.edu/alkes-price/software/

RESOURCE AVAILABILITY

Lead Contact

Further information and requests for resources and reagents should be directed to and will be fulfilled by the Lead Contact, Johannes Krause (krause@shh.mpg.de).

Materials Availability

This study did not generate new unique reagents.

Data and Code Availability

Data are available at the European Nucleotide Archive (ENA) under study accession number: PRJEB37490 (including the HBV genome recovered from individual SJN001 and the *Treponema pallidum* sub. *pertenue* genome recovered from individual SJN003).

EXPERIMENTAL MODEL AND SUBJECT DETAILS

The San José de los Naturales Royal Hospital (originally *Hospital Real de Sanct Joseph de los Naturales*) was founded between 1529 and 1531 [97–99] and dedicated to care exclusively for the indigenous population of the Viceroyalty of the New Spain. The establishment of this hospital was largely motivated by the need for medical facilities to aid the victims of the smallpox outbreaks that occurred early during the Colonial Period [100]. The vast majority of the patients were Nahuatl and Otomi speakers, which could tell us that most patients were from the central region of Mexico, including the valley of Morelos to the south and the Basin of the Balsas River to the west, as well as the boroughs of La Candelaria, Santo Tomás, San Pablo, San Antonio Abad and the towns of Jamaica and

Ixtacalco in Mexico City [22, 24]. The mortuary patterns of the archaeological context (multiple human skeletons in 13 out of 16 excavation units) suggests that most of the individuals probably died due to the epidemics that devastated Mexico City and the central plateau of New Spain which resulted in mass deaths [21, 101, 102].

Archaeological sites and sample description

Archaeological context

The samples used in this study were obtained from three individuals whose skeletons were recovered from the archaeological context of the San José de los Naturales Royal Hospital. These almost complete skeletons were recovered from the cemetery associated with the hospital during the excavations for a new subway line in downtown Mexico City between 1988 and 1994, under the supervision of the archaeologists Salvador Pulido Méndez and María de Jesús Sánchez Vázquez [21, 24]; during the season of 1992 the skeletons were found in the third stage of the excavation, suggesting they belonged to the oldest structures within the archaeological context.

Individuals and samples

Due to the possibility that these three individuals are of distinct ethnic origin (given that ethnic heterogeneity was promoted to generate social disintegration as a way to prevent the creation of communities and social organization among African slaves [2, 3, 5]). We collected one tooth from each of the following individuals: *ML8 SL 150* (age at death: 25-30 years old, male [25]; first right molar of the mandible, genomic library SJN001), *ML8 San José 214* (age at death: 30-35 years old, male (age at death: 30-35 years old, male [25]; second right molar of the maxilla, genomic library SJN002) and *ML8 SLU9B 296* (age at death: 25-30 years old, male [25]; second right molar of the mandible, genomic library SJN003). Samples were obtained under controlled conditions in the Osteology Laboratory of the Post Graduate Studies Division at the National School of Anthropology and History (ENAH) with a protocol devoted to minimize any possibility of contamination. Photographic records of the samples were obtained throughout the whole procedure. These individuals were previously described of potential African origin [6, 23, 25, 28] because of dental modifications (Figure 1) consistent with those practiced by sub-Saharan ethnic groups [25, 43, 103], as well as apparent dental and skeletal features with suggested affinity to sub Saharan human groups [26, 101]. The radiocarbon dates and strontium isotope analyses of the three individuals' samples were processed and analyzed at *The Curt-Engelhorn-Centre for Archaeometry* (Mannheim, Germany). Radiocarbon dates are reported showing the lab codes MAMS, and were processed using ultra filtrated collagen (fraction > 30kD) and dated using the *MICADAS-AMS* of the *Klaus-Tschira-Archäometrie Zentrum*. Strontium isotopes determination was performed in a high-resolution ICP mass spectrometer in a clean room laboratory at the same laboratory. Since this is quite a precise determination, as reflected by the reproducibility of NBS-987 measurements, we can confidently report and trust values to the fifth decimal place [63]. Osteological analyses were conducted on the skeletons in search for skeletal evidence of pathologies or trauma using the health indicators proposed by Goodman and Martin as well as references on osteological analyses of pathology [86, 104–106]. This methodology includes the identification of bone modifications in the skeleton present in the sites of muscle or ligament insertion caused by the hyperactivity of the main muscles responsible for the movement [107]. Dental modification patterns were assessed by comparing the dental decoration present in the SJN Africans with previously observed patterns [following the classic works by Reinaldo de Almeida (1953, 1957), as cited by references [41, 108]]. The individual biological affinity was estimated by cranial non-metric traits ancestry estimation, ranked by their degree of expression, with which percentages of biological affinity were obtained according to four biogeographical groups: Native American, African, Asian and European [109–111].

METHOD DETAILS

Osteological assessment

Osteobiography of individual ML8 SL 150 (SJN001)

Estimation of sex was performed by morphological analysis of sexually dimorphic features of the os coxa (pre-auricular sulcus, greater sciatic notch, subpubic morphology). Results indicate that this individual was likely a biologically male individual [112]. The age at death was estimated around 24 years and was obtained by analyzing the scalene tubercle and the first rib face (range of 24.28 to 51.86 years) [113]; the pubic symphysis (range: 22-25 years) [114] and the auricular surface of the ilium (range: 24-28 years) [115], which is consistent with previous estimates [25]. *Health:* The skull shows moderate cribra orbitalia and severe porotic hyperostosis. These abnormal skeletal changes are often in response to conditions associated with diet such as anemia and malnutrition, as well as parasitic infections and blood loss [38–40]. Observations investigating dental health reveal some signs of periodontal disease including receding of the alveoli with abnormal margins with associated alveolar inflammation. The tibiae and fibulae display dense sclerotic periosteal deposition suggestive of well-healed periosteal reaction. It is possible that these pathological changes are associated with conditions of poor hygiene, infectious processes, and malnutrition [40, 105, 107]. *Occupational activity:* The left clavicle presents enthesophyte development with associated raised margins at the insertion point of the coracoclavicular ligament, this may be attributed to remodelling of bone that occurs due to a microtraumas associated with repetitive use and has been reported to be found among individuals that they carry weighted loads on their shoulders [107]. The right clavicle presents exostosis in the anterolateral aspect located in the insertion of the coracoclavicular ligament (Figure S5A). The seventh thoracic vertebra presents Schmörl's node (Figure S5B) on the inferior aspect of the vertebral body resulting from the compression and subsequent hernia of inter-vertebral discs. Likewise, the ninth to the twelfth vertebrae present Schmörl's nodes on the superior and inferior aspects of the vertebral bodies. These nodes, or hernias, are the result of intense gradual compression and excessive

biomechanical stress [116]. *Cultural practices:* This individual shows dental modification in the four maxillary incisors (Figure 1 in the main text) made with two techniques: percussion fracture and filing, but also it can be seen some decoration work done in the mandibular canines [25, 107]. The patterns seen in the maxillary incisors are consistent with a "V" shaped modification present in Fang and other ethnic groups from the coastal region of central-Western Africa (present day Equatorial Guinea, northern Gabon, and southern Cameroon) [41, 43, 108]. The mandibular canines, however, present a dental modification pattern seen during 19th century expeditions in the Kingdom of Loango (present day Republic of the Congo), a multi-ethnic kingdom in the central-western part of Africa; and in Bakongo people from the Congo region [43]. *Taphonomy:* We observed green coloration on multiple skeletal elements acquired by contact with copper in the burial associated with the body. This green coloration was observed on the fifth and seventh cervical vertebra (Figure S5C) and the fourth and fifth left ribs (Figure S5D), there is a pattern of continuous inclined lines on the coloration. These indications are considered by other authors [23, 28] as a result of gun impacts. It is likely this individual had been shot and buried with the fragments in his body thus resulting in the green coloration of the skeleton. *Biological affinity:* The biological affinity of this individual was estimated from macromorphoscopic characteristics [109, 111], these characters are established by their degree of expression. For this work, the values obtained from the observation were analyzed using the software *Osteomics* [110], which bases its classification by a simple Bayesian method and proposes a probabilistic result taking into account the percentages of biological affinity according to four biogeographic groups: Native American, African, Asian and European. Individual 150 presented a large interorbital width (IOW); large nasal aperture width (NAW); as well as deep post-bregmatic depression (PBD); intermediate anterior nasal spine (ANS); inferior nasal aperture (INA) with border; a pronounced malar tubercle (MT); nasal bone contour (NBC) with intermediate plateau; supranasal suture (SPS) closed but visible; and zygomaticomaxillary suture (ZS) with an angle in the middle part; nasal overgrowth (NO) and transverse palatine suture (TPS) were not analyzed due to them being fractured. According to the classification analysis of *Osteomics*, a 92.23% probability of belonging to the African biogeographical group was found.

Osteobiography of individual ML8 San José 214 (SJN002)

The biological sex estimation of the individual was performed through observations of sexually dimorphic traits. Morphological analysis of the os coxa (preauricular sulcus, sciatic notch, composite arch, anterior edge form of the ischiopubic ramus and the ischiopubic ratio) [112] with particular attention to the morphology of the features associated with the pubic region (ventral arch, subpubic concavity, and the medial aspect of the ischiopubic ramus) resulted in the estimation of a male individual [117]. The age at death of the individual was estimated to be approximately 25 years and was calculated through age associated morphological observations of the scalene tubercle and the first rib face (range of 24.28 to 51.86 years) [113]; the pubic symphysis (range: 22-28 years) [114] and the auricular surface of the ilium (range: 25-29 years) [115]. *Health:* This individual presents signs of dental pathology including an abscess in the second lower right molar (Figure S6I), as well as periodontitis. The diaphyses of the lower limbs display periosteal deposition at the inferior most aspects. The right femora display sclerotic bone deposition creating an irregular surface which is suggestive of a healed periosteal reaction in life. Likewise, the tibiae and fibulae display periosteal reaction active at time of death; this is most apparent on the right tibia and fibula where the periosteal bone is deposited near and around the point of fracture with associated dense sclerotic and osteomyelitic bone development. *Degenerative diseases:* Degenerative disease of the joints is present and can be observed on the distal articular surface of the femur (Figure S6A) as osteochondritis dissecans, a defect of the articular surface of the bone due to compromise of the synovial capsule, and associated signs of osteoarthritis i.e., eburnation, lipping of the joint margins, and irregular joint surface [105]. Osteophytic development is present on the eighth, eleventh and twelfth thoracic vertebrae, and third and fourth lumbar vertebrae (Figure S6H); although these are age associated skeletal changes, development in younger individuals is associated with intense physical activity and excessive mechanical stress [107]. Here we see extreme osteophytic development and compression of the vertebrae. *Trauma:* Trauma refers to any sudden physical injury resulting from an external force. This individual, presents a healed fracture of the right tibia and fibula in the distal third of the diaphysis (Figures S6B–S6D) that extends from the lateral aspect to the medial aspect covered by and dense bony callus which is consistent with a healed oblique fracture and cross-section caused by the combination of axial compression force and angulation [107]. Healing of the fracture occurred without correct alignment of the fractured bones, which resulted in poor bone consolidation. The skull also presents a cut mark in the frontal bone with signs of bone regeneration (Figure S6J), which is indicative of the lesion happening ante mortem [118]. *Occupational activity:* The left and right clavicles display skeletal changes at the costoclavicular ligament, however, the right clavicle presents a higher degree of change with entheseal changes including depressed grained surface displaying raised irregular margins at the costoclavicular ligament (Figures S6E–S6G). The ulna presents enthesophyte development on the olecranon at the insertion of the triceps brachii, it is associated with continued biomechanical stress of the arm [107]. The lumbar vertebrae present Schmörl's nodes on the superior and inferior aspects of the vertebral bodies, resulting from the compression exerted on the inter-vertebral discs. In this individual, multiple Schmörl's nodes can be observed from the first to the fourth lumbar vertebrae. These vertebrae display skeletal changes (Figure S6H), as a result of an intense and gradual compression from biomechanical requirements including osteophytes on the superior and inferior surface and severe compression of the vertebra bodies in response to compression over time. The linea aspera of both femora show rugose enthesophyte development, a skeletal change associated with activity patterns; the significant enthesophytic development on the right femur is likely due to alterations in biomechanical activity resulting from the unaligned fracture of the proximal tibia and fibula. *Cultural practices:* This individual also presented dental modification in the four maxillary incisors (Figure 1 in the main text) from what appeared to be the fracture by percussion technique [107]. The patterns seen in the maxillary incisors are consistent with the "pattern No. 2" (resembling the "T" shape pattern proposed by Reichart et al. [108]) proposed by Wasterlain et al. [41], consisting in the removal of both mesial and distal incisal angles. This pattern was reported in D'zem (Njem) people, an ethnic group far to the east of the Dscha Valley (present day Cameroon) and their neighbors [43], but also

remarkably similar to that found in the individual no. 81 from the deposit of urban waste of the Valle da Gafaria (Lagos, Portugal) [41]. *Biological affinity:* The biological affinity of the individual was estimated from macromorphoscopic characteristics [109–111]. The individual shows a large interorbital width (IOW), a medium nasal aperture width (NAW), as well as deep post-bregmatic depression (PBD); small anterior nasal spine (ANS); inferior nasal aperture (INA) with a little border; a not so pronounced malar tubercle (MT); a rounded nasal bone contour (NBC); a closed but visible supranasal suture (SPS); and zygomaticomaxillary suture (ZS) with an angle in the middle part; nasal overgrowth (NO) and transverse palatine suture (TPS) were not analyzed due to them being fractured [109, 111]. According to the classification analysis of *Osteomics*, a 95.24% probability of belonging to the African biogeographical group was found.

Osteobiography of individual ML8 SLU9B 296 (SJN003)

The sex estimation of individual SJN003 was performed through morphological observations of the os coxa (preauricular sulcus, sciatic notch, composite arch, anterior edge form of the ischiopubic ramus and the ischiopubic ratio) [112] including the morphology of the pubic region (ventral arch, subpubic concavity, and the medial aspect of the ischiopubic ramus) [117]. All observations resulted in estimations of a biologically male individual. The age at death was estimated to be approximately 25.26 years and was calculated by analyzing the scalene tubercle and the first rib face [113], which is consistent with previous estimates [25]. It was not possible to obtain age using another method due to preservation issues of the pubic symphysis and the auricular surface of the ilium. *Health:* The skull presents moderate cribra orbitalia. The number of permanent teeth observed is 13 and an alveolus; abscesses or injured teeth were not present and periodontitis is observed. The presence of cribra orbitalia and hyperostosis in the skeleton can be due to three factors: diet such as malnutrition and anemia, parasitic infections, and blood loss [86]. The diaphyses of the long bones present slight infectious processes, with the exception of the femurs in which osteomyelitis can be observed on the anterior and posterior sides of the shaft (Figure S7A). Periosteal changes could be associated with a variety of physiological and environmental stressors including diet or infectious processes [86]. *Occupational activity:* The left clavicle diaphysis (Figure S7B) presents diffuse cortical irregularity and a roughened, raised appearance at the muscular insertion of the deltoid [86]. *Cultural practices:* This individual presents dental modification of maxillary and mandibular canines and central and lateral incisors (Figure 1 in the main text). The patterns seen resemble the ‘‘pattern No. 2’’ (resembling the ‘‘T’’ shape pattern proposed by Reichart et al. [108]) proposed by Wasterlain et al. [41], consisting in the removal of both mesial and distal incisal angles. This pattern was reported in D’zem (Njem) people, an ethnic group far to the east of the Dscha Valley (present day Cameroon) and their neighbors [43], and very similar to that found in the individual no. 81 from the deposit of urban waste of the Valle da Gafaria (Lagos, Portugal) [41]. *Biological affinity:* The biological affinity of the individual was estimated from macromorphoscopic characteristics [109–111]. The individual shows a large interorbital width (IOW), a medium nasal aperture width (NAW), as well as deep post-bregmatic depression (PBD); medium anterior nasal spine (ANS); inferior nasal aperture (INA) with a pronounced border; a not so pronounced malar tubercle (MT); a slightly rounded nasal bone contour (NBC) with high walls; a closed but visible supranasal suture (SPS); transverse palatine suture (TPS) goes all way through and reaches the medium line, where it projects to both the anterior and the posterior ends drawing a M shaped line; and zygomaticomaxillary suture (ZS) with an angle in the middle part; nasal overgrowth (NO) was not analyzed due to it being fractured [109, 111]. According to the classification analysis of *Osteomics*, a 91.95% probability of belonging to the African biogeographical group was found.

Stable isotope analysis, diets, and the reservoir effect

Stable isotope analysis of human bone can provide insights into the significance of different resources to the protein component of the diet, this includes the potential reliance on marine resources and their impact on ^{14}C radiocarbon measurements through the ‘reservoir effect’ [119, 120]. Here, we analyzed dentine collagen from the same teeth used to conduct the radiocarbon dating and aDNA analysis. These teeth were first (SJN001) and second molars (SJN002 and SJN003), providing dietary information for the years of tooth formation (crown-enamel formation at 2-2.5 years old for the first molar, and between 7-8 years old for the second molar) [121, 122]. Sample SJN001, as a first molar, should be treated with caution as high $\delta^{15}N$ values could be the product of breastfeeding which results in a higher trophic level appearance [34]. We obtained 250 mg of dentine powder from the crown of the analyzed teeth using a diamond-tipped drill. Collagen was then extracted from this powder using standard procedures [123]. The powder was demineralised in 10 mL aliquots of 0.5M HCl at 4°C. The acid was changed until CO_2 stopped evolving. The residue was rinsed three times in deionised water before being gelatinized in pH = 3 HCl at 75°C for 48 hours. The resulting solution was filtered, with the supernatant then being lyophilized over a period of 24 hours. After calculating the collagen yield, all purified collagen samples (1 mg) were located in tin capsules to be analyzed in duplicate at the Department of Archaeology, Max Planck Institute for the Science of Human History using a Thermo Fisher™ Elemental Analyzer coupled to a Thermo Fisher™ Delta V™ Advantage Mass Spectrometer via a ConFloIV system. Accuracy was determined by measurements of international standard reference materials within each analytical run. These were USGS40 $^{13}C_{raw} = -26.4 \pm 0.1$, $^{13}C_{true} = -26.4 \pm 0.0$, $^{15}N_{raw} = -4.4 \pm 0.1$, $^{15}N_{true} = -4.5 \pm 0.2$; IAEA N2 $^{15}N_{raw} = 20.2 \pm 0.1$, $^{15}N_{true} = 20.3 \pm 0.2$; IAEA C6 $^{13}C_{raw} = -10.9 \pm 0.1$, $^{13}C_{true} = -10.8 \pm 0.0$. The atomic C:N ratio along with the collagen yields were used in order to determine the quality of collagen preservation. Collagen yields over 1 wt% are considered acceptable for carbon and nitrogen values [124], while the C:N ratio should range from 2.9 to 3.6 [125]. Stable carbon and nitrogen isotope ratios of human tissues are expressed in δ notation relative to established international standards and shown in parts per thousand (‰). The delta values are obtained by the following equation:

$$\delta = \frac{R_{sample} - R_{standard}}{R_{standard}} \times 1000$$

where the R represents the ratio between the heavier (^{13}C, ^{15}N) and lighter (^{12}C, ^{14}N) isotopes [126]. $\delta^{13}C$ and $\delta^{15}N$ analysis of human bone collagen primarily reflects the isotopic values of the protein input to the diet, with minimal contribution of lipids and carbohydrates, meaning that it will be heavily influenced by protein-rich foods [127].

Stable carbon isotope variability in terrestrial ecosystems is primarily driven by two dominant photosynthetic pathways, C_3 and C_4, which differ in their net discrimination against ^{13}C during CO_2 fixation [128]. In C_3 plants, strong discrimination against ^{13}C results in lower ^{13}C values in virtually all trees, shrubs, and temperate grasses, including wheat, than in C_4 plants such as maize and millet [129]. C_3 ^{13}C values vary from *c.* −24 to −36‰ (global mean −26.5‰), while C_4 values range from *c.* −9 to −17‰ (global mean −12‰) [129]. C_3 and C_4 plants thus have distinct and non-overlapping ^{13}C values [130]. These distinctions are reflected in the tissues of consumers, with small trophic level effects of 1-2‰ [127].

Stable nitrogen isotope ratios vary with tropic level, and ^{15}N trophic shifts of +2-6‰ from plants to herbivores, and from herbivores to carnivores, is well documented in marine and terrestrial systems [35, 131]. This trophic effect is most likely linked to the loss of ^{15}N-depleted excretion products [132], although diet-tissue distinctions are highly variable between animals [133]. The long length of marine food chains, leads to distinctively high ^{15}N in marine foods and consumers compared to their terrestrial counterparts [134]. Freshwater foods also tend to have high ^{15}N though ^{13}C does not follow the same trend toward higher measurements as in marine food chains due to different sources of carbon dioxide for primary producers [135].

Despite the long history of stable isotope research in African archaeology, there is a significant inequality in the application of these studies across the regions of Africa [36]. While South and East Africa have been well covered, other regions, especially West Africa, remain relatively unexplored [36]. In the context of 16th-19th century slavery, historical records are often lacking in terms of insights into the origins of enslaved individuals and their subsistence strategies, focusing on coastal embarkation points into the Atlantic Trade rather than places of residence which may, in many cases, have been hundreds of kilometres away [136]. Stable carbon and nitrogen isotope analysis of 16th-19th century slave populations in southern Africa [137] and the Caribbean [67] have already shown the efficacy of this methodology for uncovering insights into individual origins.

In the context of 16th-19th West Africa, stable isotopic insights into broad subsistence bases may also provide geographic information. For example, along the west coast there was a well-documented focus on rice (C_3) [138], in the south of Ghana there was a greater focus on yams and other root crops (C_3), and in the semi-arid interior there was often a contribution of C_4 crops such as sorghum and millet [139]. Thus, the different regional agriculture techniques of subsistence may be useful in establishing the origin of those individuals enslaved in the West of Africa [67]. That said, existing isotopic information from slaves of African origin in the Americas indicate an adult diet of C_4 crops and marine resources [64, 67, 140, 141]. This is particularly significant in our context given its potential influence on establishing a secure chronology for human remains.

Marine and freshwater environments are reservoirs of ^{14}C. This means that in a marine or freshwater environment, ^{14}C concentrations in CO_2 are lower than contemporary atmospheric values, leading to 'older' radiocarbon dates in those organisms relying on freshwater or marine systems [142]. Aquatic plants and phytoplankton fix this CO_2, transferring relatively low concentrations of ^{14}C up the foodchain. The direct or indirect consumption of marine proteins by human beings will thus impact ^{14}C measurements of their tissues, making them seem 'older' through the marine reservoir effect [143–145]. Thus, before the conversion of the radiocarbon date results to a calendar age, it is important to determine the degree of marine consumption in an individual.

Ancient DNA sample processing and quality control

Sampling

All samples were processed in dedicated laboratories at the Max Planck Institute for the Science of Human History in Jena, Germany. Tooth powder (~80 mg) was obtained by cutting each dental piece at the junction between the root and crown and sampling the dental pulp from the crown (*A libraries*) and the root (*B libraries*). These procedures were carried out after a bleach/rinse and UV decontamination protocol. After sampling, the remaining root was used for radiocarbon dating, while the crown was sampled for Sr determinations as previously described.

DNA extraction

DNA was obtained from bone powder after overnight extraction at 37°C with a decalcifying buffer (900 μL EDTA 0.5M, 75μL H_2O and 25 μL Proteinase K) [146]. The whole mixture was then centrifuged to pellet the remaining tooth powder and the liquid transferred into a binding buffer as previously described [147]. DNA was then purified by a silica column-based method using silica columns for high volumes (*High Pure Viral Nucleic Acid Large Volume Kit*, Roche Molecular Systems, Inc.; Pleasanton, CA). DNA was eluted in TET (10mM Tris, 1mM EDTA and 0.05% Tween) in two 50 μL-steps for a final volume of 100 μL and frozen at −20°C until library preparation. Negative blanks and cave bear positive controls were included for each step of the procedure.

Library preparation

We built one non-uracil DNA glycosylase (non-UDG) treated library using 15 μL of each DNA extract to assess the authenticity of the extracted DNA after obtaining the characteristic damage plots associated with ancient DNA [148]. We then used 20 μL of each DNA extract to build UDG-half libraries with *Illumina*-specific adapters following a modified double-stranded library preparation protocol as previously described [149, 150]. Each library was treated independently despite being from the same individual. Libraries were quantified using qPCR with the IS7 and IS8 primers in a quantification assay using a *DyNAmo SYBR Green qPCR Kit* (Thermo Fisher

Scientific Inc.; Waltham, MA) on the *LightCycler® 96* (Roche Diagnostics Inc.; Risch-Rotkreuz, Switzerland). Each library was identified with the respective pair of indexes in double-100 μL reactions using *PfuTurbo DNA Polymerase* (Agilent Technologies, Inc.; Santa Clara, CA). The indexed products for each library were pooled, purified over silica columns using the *MinElute PCR Purification Kit* (QIAGEN N.V.; Hilden, Germany), eluted in 44 μL TET and again qPCR quantified, now using the IS5 and IS6 primers. Conditioning for sequencing included the amplification of the purified product in 4x100 μL reactions using *Herculase II Fusion DNA Polymerase* (Agilent Technologies, Inc.; Santa Clara, CA) following the manufacturer's specifications with 0.3 μM of each IS5/IS6 primers, following a purification over silica columns also using the *MinElute PCR Purification Kit*, and elution in a final volume of 22 μL TET. Two microliters of the conditioned product were diluted 1:10 and quantified using the *Agilent 2100 Bioanalyzer DNA 1000* protocol (Agilent Technologies, Inc.; Santa Clara, CA). An equimolar (10mM final concentration) pool of all libraries was then prepared for shotgun sequencing on the *Illumina HiSeq 4000 Systems* platform (Illumina, Inc., San Diego, CA). Both libraries of each individual were sequenced to 5 million reads depth to obtain basic QC parameters with the aid of the *EAGER* pipeline ver. 1.92.55 [90] and decided for either deeper sequencing or in-solution capture.

Whole-genome and immune-genes captures

Using in-solution capture based on modified immortalized probe sequences [151], target immunity genes sequences or a panel of around 1,237,207 single nucleotide polymorphisms (SNPs) were enriched via in-solution capture from the total DNA in the sequencing libraries [152–154]. Briefly, UDG-half- treated libraries were re-conditioned by further amplifying with IS5/IS6 primers and *Herculase II Fusion DNA Polymerase* to reach a concentration of 200–400 ng/μL as measured on a *NanoDrop 8000* spectrophotometer (Thermo Fisher Scientific Inc.; Waltham, MA). Capture was performed on 5.25 μL of each re conditioned library using that volume for each capture procedure [153, 154]. After enrichment, captured library pools were paired-end sequenced on the *Illumina Hiseq 4000* (Illumina, Inc., San Diego, CA) with 75 single-end cycles providing on average 10 million reads per sample. *Illumina* sequencing adapters were removed by demultiplexing, which was performed by sorting all the sequences corresponding to their respective indices using the *bcl2fastq Conversion Software* ver. 2.17.1.14 and *dnaclust* ver. 3.0.0 [155].

Immune-genes capture design

We designed a set of enrichment probes for 488 human genes part of both the innate and adaptive immune system [156]. Exon sequences for these genes were extracted from the human genome build *hg19* [29] using the *RefSeqGene* records from the NCBI/Nucleotide database [157]. Introns were also used in the case of MIC genes. Given the polymorphic nature of these genes, we added alternative alleles for HLA, MIC, TAP and KIR genomic regions, which were obtained from the IMGT/HLA database [158]. For HLA class I and KIR genes the intronic regions were also included. For the HLA and MIC genes a set of 83 representative alleles with full-length gene sequences was chosen that encompasses the major allelic groups [159] and covers 95% of the known polymorphism. To capture the remaining 5%, a set of 162 × 160 base pairs (bp) consensus sequences was designed. A 60-bp probe set was designed at every 5bp interval along the target sequences. The final 52-bp probe sequences were mapped to *hg19* using RazerS3 [160] with a minimum threshold of 95% identity. The probe set was tripled to complete capacity of the one-million feature SureSelect DNA Capture Array, which was turned into an in-solution DNA capture library as described elsewhere [153]. We enriched the reads mapping to the HLA region with the described in-solution capture approach, yielding 10X-100X coverage for this genomic region. For dealing with the allele assignation coming from short reads, we used Optitype [54], a software specifically developed to deal with short reads coming from ancient DNA data. Our capture approach was validated using previously typed samples coming from an external quality control program (UCLA's International HLA DNA Exchange), for which the DNA was shredded using the Covaris system to provide short DNA fragments for a proper validation of the results. The fact that the alleles typed in our individuals are commonly found in Sub-Saharan African populations further supports our findings.

Treponema pallidum capture design

For targeted enrichment of *Treponema pallidum* DNA probes were designed on the basis of *Treponema pallidum* subsp. *pallidum*, *T. pallidum* subsp. *endemicum* and *T. pallidum* subsp. *pertenue* strains. The probes were designed with a 1bp tiling and a length of 52 bp with an additional 8bp linker sequence (CACTGCGG) as described previously [153]. Duplicated probes and probes with low sequence complexity were removed. This resulted in 1,125,985 unique probe sequences. This probe set was spread on two Agilent one-million feature SureSelect DNA Capture Arrays. The capacity of the two arrays was filled by randomly duplicating probes from the probe set. The arrays were turned into an in-solution DNA capture library as described elsewhere [153].

List of Treponema pallidum genomes IDs used for probe design

Treponema pallidum subsp. *pallidum* strains Nichols (NC_000919.1), SS14 (NC_021508.1), Sea 81-4 (NZ_CP003679.1), Mexico A (NC_018722.1), *T. pallidum* subsp. *endemicum* strain Bosnia A (NZ_CP007548.1), and *T. pallidum* subsp. *pertenue* strain Fribourg-Blanc (NC_021179.1).

Hepatitis B Virus (HBV) capture design

For targeted HBV DNA enrichment, probes were designed on the basis of a worldwide set of HBV full genomes (see list of GenBank accessions below). The probes were designed with a 1bp tiling and a length of 52 bp with an additional 8bp linker sequence (CACTGCGG) as described previously [153]. Duplicated probes and probes with low sequence complexity were removed. This resulted in 221,190 unique probe sequences. This probe set was replicated four times on an Agilent one-million feature SureSelect DNA Capture Array, which was turned into an in-solution DNA capture library as described elsewhere [153].

List of HBV genome IDs used for probe design

Petersberg, Sorsum, Karsdorf, LT992459, LT992455, LT992454, LT992448, LT992447, LT992444, LT992443, LT992442, LT992441, LT992440, LT992439, LT992438, JN315779, MG585269, AB076679, AB116084, AB453988, AY738142, GQ477499, AY934764,

FJ692556, FJ692598, FJ692611, GQ161813, GQ331046, AB073858, AB033555, AB219429, AB219430, AP011089, AB073835, AB287316, AB287318, AB287320, AB287321, DQ463789, DQ463792, AB241117, DQ993686, AB111946, AB112066, AB112472, DQ089767, X75656, X75665, AB048704, AB048705, AF241411, AP011100, AP011102, AP011103, AP011106, AP011108, FJ899792, JN642140, GQ477453, GQ477455, JN642160, JN642163, JN688710, JN688711, GQ922005, HE974378, KJ470893, KJ470896, KJ470898, FJ904430, FJ904436, AB033559, AB048701, AB048702, AB188243, AB210818, AM494716, AY796031, AY902768, DQ315779, X80925, X75657, X75664, AY090458, AB116654, FJ657525, AY090455, AY311369, DQ899144, DQ899146, AB116549, X75663, AF223962, AB166850, AB056513, AB064312, AF405706, AB059660, AB375163, AY090454, AY090457, AB486012, AY330911, AJ131571, AY781180, U46935, AJ131567, AF193863, EU155824, KC790378, KC790377, KC790376, NC_001484, U29144, NC_004107, AF046996, KY703886, MH307930, AF498266.

Pathogen genome capture

After finding reads mapping to HBV (SJN001) and *Treponema pallidum* (SJN003), we selectively enriched for these pathogens in their respective libraries. Using in-solution capture based on modified immortalized probe sequences [153], target pathogen genomes were enriched via in-solution capture from the total DNA in the sequencing libraries [152–154]. Briefly, UDG-half- treated libraries were reconditioned by further amplifying with IS5/IS6 primers and *Herculase II Fusion DNA Polymerase* to reach a concentration of 200–400 ng/μL as measured on a *NanoDrop 8000* spectrophotometer (Thermo Fisher Scientific Inc.; Waltham, MA). Capture was performed on 5.25 μL of each re-conditioned library using that volume for each capture procedure [153, 154]. For targeted HBV and *Treponema* genome DNA enrichment, we used the previously described sets of probes. After enrichment, captured library pools were paired-end sequenced on the *Illumina Hiseq 4000* (Illumina, Inc., San Diego, CA) with 75 cycles providing on average 10 million reads per sample for the first round of capture and 20 million (*Treponema*) and 13 million (HBV) reads per sample for the second round of capture.

QUANTIFICATION AND STATISTICAL ANALYSIS

QC and data processing for human PopGen

We performed an analysis of the human captured sequence data using *EAGER* ver. 1.92.55 [90]. Clip&Merge [90] and *AdapterRemoval* v.2 [88] were used to trim adaptor sequences and to remove adaptor dimers and low-quality sequence reads (min length = 30; min base quality = 20) from the reads resulting from the sequencing of the aDNA libraries. Pre-processed sequences were mapped to the human genome assembly GRCh37 (hg19) from the Genome Reference Consortium [29] using *BWA* ver. 0.7.12 [89] and a default seed length of 32.

aDNA Authentication

The C to T misincorporation frequencies typical of aDNA were obtained using *mapDamage* 2.0 [92] to assess the authenticity of the ancient DNA fragments from the non-UDG treated libraries. Characteristic short average fragment length (49-55 base pairs) and the increased proportion of miscoding lesions due to deamination at the molecule extremes were found on the six UDG-half libraries analyzed (Table S2).

Data processing

Duplicates were removed with *DeDup* [90], which removes identical reads. UDG-half libraries were trimmed for the first and last three positions to reduce the impact of deamination-induced misincorporations during genotyping. We used *samtools mpileup* (parameters –q 30 –Q 30 –B) to generate a pileup file from the merged sequence data of each individual, and used a custom script [*pileupCaller* ver. 8.2.2 [161]] to genotype the individuals, using a pseudo-haploid random draw approach. For each position on our capture panel, a random read was drawn for each individual and the allele of that read was assumed to be the homozygous genotype of the individual at that position. In order to compare with available data from African populations, were merged our SNPs to the approx. 600,000 SNPs of the Human Origins dataset [30]. Genetic sex of the three samples was assigned using SNP capture data by calculating the ratio of average X chromosomal and Y chromosomal coverage to average autosomal coverage at the targeted SNPs [31]. Samples with an X rate between 0.35 and 0.55 and a Y rate between 0.4 and 0.7 were confirmed male. Since the three analyzed individuals were male, *ANGSD* was run to measure the rate of heterozygosity of polymorphic sites on the X chromosome after accounting for sequencing errors in the flanking regions to estimate the nuclear contamination, since males are expected to have only one allele at each position [32]. Reads mapping to the human mitochondrial DNA (mtDNA) were used to reconstruct a mtDNA consensus sequence and estimate contamination levels with *schmutzi* [33]. Present-day human contamination estimates were performed using a comparative database of 197 modern-day worldwide mtDNA sequences provided with the software package. After assessing the quality of the independent libraries, libraries A and B of each individual were merged using *SAMtools* ver. 1.3 [94].

Uniparental markers

Mitochondrial DNA (mtDNA) genomes were determined mapping reads to the revised Cambridge reference sequence [162]. For the resulting sequences, we filtered positions with likelihoods above 10, 20 or 30 and used *HaploGrep2* [163] and *HAPLOFIND* [164] to assign and confirm the corresponding mtDNA haplogroups. The aligned mtDNA genomes were compared to other available genomes from literature which belong to one of the three haplogroups retrieved (153 sequences for L1b, 208 for L3d and 415 for L3e). The mtDNA sequences were aligned with MAFFT (http://mafft.cbrc.jp/alignment/software/) [165] and manually checked with Bioedit (http://www.mbio.ncsu.edu/BioEdit/bioedit.html). The two poly-C regions (positions: 303–315, 16,183–16,194) were excluded from the analysis. Haplotype based networks (Figure S1) were built with R with the command haploNet of package PEGAS [166]. Sequenced reads mapped to Y-Chromosome (Y-Chr) SNPs within our capture panel that are also present in the Y-DNA

Haplogroup Tree 2018 ver. 13.174 [167] were used to assign Y-Chr haplogroups for each individual. Haplogroup assignment was manually confirmed by looking at the most downstream SNP retrieved after assessing the presence of upstream mutations along the Y-Chr haplogroup phylogeny.

Principal components analysis

smartpca (version 16000) from the *Eigensoft* package [168] was used to calculate Principal Components (PCs) of variation in the present-day populations from the HO dataset, using the options "lsqproject: YES" and "shrinkmode: YES." Initially, we projected the three ancient individuals on PCs calculated on the genetic variation in 371 worldwide populations, to access the continental-level ancestries in the ancient individuals (Figure S2). We then projected the ancient individuals on PCs calculated on variation from 534 Africans from 51 populations, both from Northern and sub-Saharan Africa (Figures 2 and S2).

Worldwide populations

Abazin, Abkhasian, Adygei, Afar WGA, Ain Touta WGA, Albanian, Aleut, Aleut Tlingit, Algerian, Algonquin, Altaian, Altaian Chelkans, Ami, Apalai, Arara, Argentina Puna, Armenian, Armenian Hemsheni, Assyrian, Atayal, Australian WGA, Australian, Avar, Aymara, Azeri, Azeri WGA, Baalberge MN, Balkar, Balochi, Bantu Herero, Bantu Kenya, Bantu SA, Bantu SA Herero, Bantu SA Ovambo, Bantu Tswana, Bashkir, Basque, Bedouin A, Bedouin B, Belarusian, Bengali, Bergamo, Berry Au Bac, Besermyan, Biaka, Bichon, Bockstein published, Bolivian, Borneo, Bougainville, Brahmin Tiwari, Brahmin, Brahui, Brillenhohle, Bulgarian, Burbur WGA, Burmese, Burusho, Buryat, Cabecar, Cambodian, Canary Islander, Chane, Chaudardes1, Chechen, Chilote, Chipewyan, Choiseul, Chukchi, Chuvash, Circassian, Cree, Crete, Croatian, Cypriot, Czech, Dai, Damara, Darginian, Datog, Daur, Dinka, Dolgan, Druze, Dungan, Dusun, Egyptian, Enets, English, Esan, Eskimo Chaplin, Eskimo Chaplin Sireniki, Eskimo Naukan, Eskimo Sireniki, Estonian, Even, Evenk FarEast, Evenk Transbaikal, Ezid, Falkenstein, Finnish, French, Fuego Patagonian.SG, Gagauz, Gambian, Gana, Georgian, Georgian WGA, Georgian, German, Greek, Greek WGA, Guarani, Guarani GN, Guarani KW, Gui, Gujarati A, Gujarati B, Gujarati C, Gujarati D, Hadza, Hadza1, Haiom, Han, Hawaiian, Hazara, Hezhen, Himba, Hoan, Hungarian, Icelandic, Igbo, Igorot, Inga, Ingushian, Iran contemporary, Iran Zoroastrian, Iranian, Iraqi Jew, Irish, Irish Ulster, Irula, Italian North, Italian South, Itelmen, Japanese, Jew Ashkenazi, Jew Cochin, Jew Ethiopian, Jew Georgian, Jew Iranian, Jew Iraqi, Jew Libyan, Jew Moroccan, Jew Tunisian, Jew Turkish, Jew Yemenite, Jordanian, Ju Hoan North, Ju Hoan South, Kabardinian, Kaitag, Kalash, Kalmyk, Kapu, Kaqchikel, Karachai, Karaim, Karakalpak, Karelian, Karitiana, Kazakh, Ket, Kgalagadi, Khakass, Khakass Kachins, Khamnegan, Kharia, Khomani, Khwe, Kikuyu, Kinh, Kirghiz, Kolombangara, Kongo, Korean, Koryak, Kotias, Kubachinian, Kumyk, Kurd, Kurumba, Kusunda, Kyrgyz, Lahu, Lak, Lapita Tonga, Lebanese, Lebanese Muslim, Lemande, Lezgin, Libyan, Lithuanian, Lodhi, Loschbour, Luhya, Luo, Makira, Makrani, Mala, Malaita, Maltese, Mamanwa, Mandenka, Mansi, Maori, Masai, Mayan, Mbuti, Mende, Miao, Mixe, Mixtec, Moldavian, Mongol, Mongola, Mordovian, Moroccan, Mozabite, Mycenaean, Nahua, Nama, Nanai, Naro, Nasioi, Naxi, Negidal, New Guinea, Nganasan, Nggela, Nivh, Nogai, Norwegian, Oase1, Ojibwa, Okunevo.SG, Onge, Ontong Java, Orcadian, Oromo, Oroqen, Ossetian, Ostuni1, Palestinian, Papuan, Papuan Central, Papuan Gulf, Pathan, Piapoco, Pima, Polish, Poltavka, Potapovka, PPNB, PPNC, Punjabi, Quechua, Ranongga, Relli, Remedello BA, Rennell and Bellona, Rochedane published, Romanian, Russell, Russian, Russian Archangelsk Krasnoborsky, Russian Archangelsk Leshukonsky, Russian Archangelsk Pinezhsky, Saami WGA, Saharawi, Samaritan, Sandawe, Santa Cruz, Santa Isabel, Sardinian, Satsurblia, Saudi, Savo, Saxon, Scottish, Scythian IA, Selkup, Semende, Shaigi WGA, She, Sherpa, Shetlandic, Shor Khakassia, Shor Mountain, Shua, Sicilian, Sindhi Pakistan, Somali, Sorb, Spanish, Spanish North, Srubnaya, Stuttgart, Surui, Sweden IA.SG, Syrian, Taa East, Taa North, Taa West, Tabasaran, Tajik, Tatar Astrakhan, Tatar Crimean, Tatar Kazan, Tatar Mishar, Tatar Siberian, Tatar Siberian Zabolotniye, Thai, Tibetan, Ticuna, Tikopia, Tlingit, Todzin, Tongan, TRB Sweden MN.SG, Tshwa, Tswana, Tu, Tubalar, Tujia, Tunisian, Turkish, Turkish Balikesir, Turkmen, Tuscan, Tuvinian, Udmurt, Ukrainian, Ulchi, Urubu Kaapor, Uygur, Uzbek, Uzbek WGA, Vatya.SG, Vella Lavella, Veps, Vestonice13, Vishwabrahmin, Wambo, Wayuu, Xavante, Xibo, Xibo, Xuun, Yadava, Yakut, Yemeni, Yemenite Jew, Yi, Yoruba, Yukagir, Zapotec, Zoro.

African and related populations

Algerian, Bantu (Kenya), Bantu (South Africa), Bantu (Herero), Bantu (Ovambo), Bedouin A, Bedouin B, Biaka, Canary Islander, Damara, Datog, Dinka, Egyptian, Esan, Gambian, Gana, Gui, Hadza, Haiom, Himba, Hoan, Igbo, Ethiopian Jew, Libyan Jew, Moroccan Jew, Tunisian Jew, Ju hoan (North), Ju hoan (South), Kgalagadi, Khomani, Khwe, Kikuyu, Kongo, Lemande, Libyan, Luhya, Luo, Mandenka, Masai, Mbuti, Mende, Moroccan, Mozabite, Nama, Naro, Oromo, Saharawi, Sandawe, Shua, SJN, Somali, Taa East, Taa North, Taa West, Tshwa, Tswana, Tunisian, Wambo, Xuun, Yoruba.

ADMIXTURE analysis

We used ADMIXTURE ver. 1.3.0 [169], a maximum-likelihood based clustering algorithm to estimate the genetic structure present in our samples, after excluding variants with minor allele frequency of 0.01 and following LD pruning using Plink (ver. 1.90) with a step size of 5, a window size of 200, and an R2 threshold of 0.5 [170]. For K = 2 to K = 14, we estimated the cross-validation (CV) error with 100 bootstrap replicates in an unsupervised model using a panel of 66 populations, including two European (Spanish and French), two Asian (Han and Cambodian), one Oceanian (New Guinea) and two Native American (Mixe and Zapotec) populations to account for different probable sources of genetic contribution in the context of the colonial period in Mexico [2, 5, 6, 26, 101, 168, 171] to assess whether the analyzed individuals had traces of admixture from non-African parental populations (Figure 2). The lowest CV error corresponded to K = 10.

Population dataset for ADMIXTURE

Algerian, Bantu (Kenya), Bantu (South Africa), Bantu (Herero), Bantu (Ovambo), Bedouin A, Bedouin B, Biaka, Cambodian, Canary Islander, Damara, Datog, Dinka, Egyptian, Esan, French, Gambian, Gana, Gui, Hadza, Haiom, Han, Himba, Hoan, Igbo, Ethiopian Jew, Libyan Jew, Moroccan Jew, Tunisian Jew, Ju hoan (North), Ju hoan (South), Kgalagadi, Khomani, Khwe, Kikuyu, Kongo,

Lemande, Libyan, Luhya, Luo, Mandenka, Masai, Mbuti, Mende, Mixe, Moroccan, Mozabite, Nama, Naro, New Guinea, Oromo, Saharawi, Sandawe, Shua, SJN, Somali, Spanish, Taa East, Taa North, Taa West, Tshwa, Tswana, Tunisian, Wambo, Xuun, Yoruba, Zapotec.

F_3 and D tests

To assess the genetic relationships and admixtures suggested in the PCA and ADMIXTURE analysis, we carried out *F*-statistics using the programs qp3Pop ver. 412 and qpDstat ver. 711 in the ADMIXTOOLS suite [172] for F_3- and D-statistics, respectively. We tested each individual independently, as they most probably were of different ancestries as explained before. We used a F_3-statistics of the form f_3 (*Outgroup*; *X*,*Y*) to measure the amount of shared genetic drift of populations *X* and *Y* after their divergence from a non-African outgroup (Figure 3); were *X* is each of the SJN individuals, *Y* is each of the populations in our database, and *Outgroup* is the genome of the Ust'-Ishim individual [62]. D-statistics of the form *D* (*Chimp*, SJN00*X*; *Y*, *Target*) were used to demonstrate if our African individuals are related to a target population or shared an excess of alleles with any population in position *Y*. A negative value implies that either *Chimp* and *Target*, or *SJN* and *Y* share more alleles than expected under the null hypothesis of a symmetrical relationship between *Y* and *Target*. Target was each of the populations with the highest top F_3 values for each SJN individual. For SJN001 (Figure S3A) Mende were used as Target; for SJN002 (Figure S3B), Bantu-speaking Ovambo were used as Target; for SJN003 (Figure S3C) Lemande were used as Target. To test for cladality between each of the individuals from SJN and their respective Target populations, we computed *D* statistics of the form *D* (*Chimp*, *X*; *Target*, *SJN00X*). We find that none of the ancient individuals are truly cladal with the *Target* populations (Table S1).

Pathogen genomes assemblies

Hepatitis B Virus genome

After HBV DNA capture and sequencing, resulting reads were merged and aligned against an HBV genome (GenBank accession: KC875253) using Geneious v. 9 with medium sensitivity settings. A 90% consensus sequence was generated with a coverage threshold of 3x. Reads were remapped against the consensus sequence within the Eager pipeline [90] to perform final coverage and damage assessment. The sequence was aligned with a worldwide set of HBV full genomes (see accession numbers below), using MAFFT [165]. The alignment was cleaned using Gblocks [173], removing positions with more than 50% gaps. A phylogenetic tree was constructed using RAxML v. 8 [174] with GTRCAT substitution model and the rapid bootstrap algorithm (Figure 4).

Treponema pallidum sub. pertenue genome and phylogenetic analyses

Shotgun reads sequenced from both libraries of SJN003 were screened for pathogens in MALT [175]. Reads mapping to *Treponema pallidum* were identified and their ancient origin was validated from deamination of cytosine to thymine bases at the reads' ends. A whole genome-wide capture with the probes described above was performed to enrich for DNA fragments of treponemal species. Paired-end reads from reference genomes; ancient genomes reads from individuals 94B and 133 from the ex-Convent of Santa Isabel from colonial Mexico [71] and reads from second round of enrichment of the SJN003 libraries were processed in EAGER (version 1.92.7) [90]. Additionally, simulated reads (100bp length with 99bp overlap to successive reads) from complete genomes of *Treponema pallidum* downloaded from NCBI were analyzed. Adapters and poor quality (minimum base quality of 20 and sequence length of 30) reads were filtered out. Both simulated and sequenced reads were mapped against *Treponema pallidum* sub. *pallidum* Nichols reference genome (GenBank accession number: NC_021490.2) using BWA ver. 0.7.12 [89] for a seed length of 32, a 0.1 mapping stringency setting (-n) and mapping quality of 37 followed by exclusion of duplicated reads using Mark Duplicates [176]. GATK identified genotypes for all sites and variants were estimated. Variants from all *vcf.* files were compared and combined for reference Nichols genome using MultiVCFAnalyser v. 0.87 (https://github.com/alexherbig/MultiVCFAnalyzer [177]). For each position, an allele is called if covered by a minimum of three reads, having a mapping quality of 30 and a frequency of 90% or greater among all reads covering the position. Otherwise, the position is considered as "N." All variant sites are concatenated to a SNP alignment. Additionally, a genome wide alignment with respect to the reference genome was created (Table S3).

To compare the ancient and modern treponemal genomes, a genome wide alignment and concatenated SNP alignment of *Treponema pallidum* sub. *pallidum* (n = 5), *Treponema pallidum* sub. *endemicum* (n = 2) and *Treponema pallidum* sub. *pertenue* (n = 26) genomes was generated. A maximum likelihood tree was reconstructed using RAxML [174], for 1000 replicates with a GTR model of substitution and a GAMMA distribution of rate heterogeneity model for eight categories. SNPs in SJN003 and 133 were analyzed in comparison to other treponemal genomes in order to identify private variants, variants shared between the two genomes and variants that appear to be homoplastic (Table S3). We identified regions of recombination in the genome wide alignments using ClonalFrameML ver. 1.-178 (https://github.com/xavierdidelot/ClonalFrameML [178]) given the maximum likelihood tree with default parameters. The three homoplastic SNPs observed in SJN003 and sites of recombination were excluded from the genome wide alignment and a Maximum Likelihood tree was reconstructed as described above (Figure 5).

List of HBV genomes GenBank accession numbers used in the phylogenetic analysis

AB076679, AB116084, AB453988, AY738142, GQ477499, AY934764, FJ692556, FJ692598, FJ692611, GQ161813, GQ331046, AB073858, AB033555, AB219429, AB219430, AP011089, AB073835, AB287316, AB287318, AB287320, AB287321, DQ463789, DQ463792, AB241117, DQ993686, AB111946, AB112066, AB112472, DQ089767, X75656, X75665, AB048704, AB048705, AF241411, AP011100, AP011102, AP011103, AP011106, AP011108, FJ899792, JN642140, GQ477453, GQ477455, JN642160, JN642163, JN688710, JN688711, GQ922005, HE974378, KJ470893, KJ470896, KJ470898, FJ904430, FJ904436, AB033559, AB048701, AB048702, AB188243, AB210818, AM494716, AY796031, AY902768, DQ315779, X80925, X75657, X75664, AY090458, AB116654, FJ657525, AY090455, AY311369, DQ899144, DQ899146, AB116549, X75663, AF223962, AB166850,

AB056513, AB064312, AF405706, AB059660, AB375163, AY090454, AY090457, AB486012, AY330911, AJ131571, AY781180, U46935, AJ131567, AF193863, EU155824, FJ899779, AB049609, FJ904399, AY721612, AY741797, AB270543, EU594409, AB109476, AB555496, GQ205377, HM363593, JN792922, AB562463, FJ023669, EU835241, AY934764.

List of Treponema spp. genomes used in the phylogenetic analysis

133 (from Santa Isabel, colonial Mexico [71]), A10, A12, IGU, Bosnia_A, CDC 2575, CDC-2, CDC-1, Fribourg-Blanc, Gauthier, Ghana-051, HATO, Iraq B, Kampung Dalan K363, LMNP-1, M2, M3, Nichols, Sea81-4, ERS945418, ERS945420, ERS945424, ERS945426, ERS945430, ERS945436, ERS945437, ERS945442, Samoa D, Sei Geringging K403, SS14, Mexico A, 94B (from Santa Isabel, colonial Mexico [71]).